Research on the electromagnetic and weak dipole moments of the tau-lepton at the Bestest Little Higgs Model

E. Cruz-Albaro*,[1] A. Gutiérrez-Rodríguez†,[1] J. I. Aranda,[2] and F. Ramírez-Zavaleta[2]

[1]*Facultad de Física, Universidad Autónoma de Zacatecas*

Apartado Postal C-580, 98060 Zacatecas, México.

[2]*Facultad de Ciencias Físico Matemáticas,*

Universidad Michoacana de San Nicolás de Hidalgo

Avenida Francisco, J. Mújica S/N, 58060, Morelia, Michoacán, México.

(Dated: November 26, 2022)

Abstract

In this paper, using the Bestest Little Higgs Model (BLHM) we calculate at the one-loop level the contributions to the Anomalous Magnetic Dipole Moment (AMDM) and Anomalous Weak Magnetic Dipole Moment (AWMDM) of the tau-lepton. The implications from this model are studied, emphasizing the contributions of the new physics induced by the new scalar and vector bosons of the BLHM: $S_i = H_0, A_0, \phi^0, \eta^0, \sigma, H^{\pm}, \phi^{\pm}, \eta^{\pm}$, and $V_i = Z', W'^{\pm}$ because these quantify the new physics. With these new contributions, we estimated bounds on the real and imaginary parts of the AMDM and AWMDM of the tau-lepton. Our study complements other one-loop-level research performed on models beyond the Standard Model.

PACS numbers: 14.60.Fg, 12.60.-i

Keywords: Taus, Models beyond the Standard Model.

* elicruzalbaro88@gmail.com

† alexgu@fisica.uaz.edu.mx

I. INTRODUCTION

The study of the physics of the tau-lepton by the ATLAS and CMS experiments [1–5] at the Large Hadron Collider (LHC) has developed significantly and now represents a very active physics program. In addition, the following present and future colliders: hadron-hadron (pp), lepton-hadron (e^-p), and lepton-lepton (e^+e^-, $\mu^+\mu^-$) for the post LHC era will open up new horizons in the field of fundamental physics. All of these colliders contemplate in their physics programs the study of the physics of the tau-lepton.

In the Standard Model (SM) of elementary particle physics, as well as in many of its extensions, the search for Anomalous Magnetic Dipole Moments (AMDM), Electric Dipole Moments (EDM), and Anomalous Weak Magnetic Dipole Moments (AWMDM) of fundamental fermions, and in particular from the tau-lepton is an essential aspect of theoretical, phenomenological and experimental investigations hunting for physics beyond the Standard Model (BSM) of particle physics. For a review of the bounds on the electromagnetic and weak dipole moments, see Refs. [6–20].

In the lepton sector, the tau-lepton is a key particle in the SM and several extensions of the SM as it is considered a laboratory for many experimental or simulation aspects of the search for new physics. This particle is characterized by its high mass [21] compared to the mass of the electron or muon, so one would expect its electromagnetic and weak dipole moments to be much more sensitive to the effects of new physics than the electron or muon itself [19]. Unfortunately, the very short τ lifetime [21] makes it very difficult to measure its dipole moments (AMDM, EDM, AWMDM) with a precision good enough to perform a significative test. The spin-precession technique adopted in the electron and muon $g-2$ is no-longer feasible [19]. Instead, one measures the production of tau pairs at different high-energy processes. For instance, the most stringent current bound on the τ AMDM (see Table I) was derived using the data collected by the DELPHI Collaboration from measurements in the cross-section of the process $e^+e^- \to e^+e^-\tau^+\tau^-$ at $\sqrt{s}$ between 183 and 208 GeV at LEP2 [22]. As for the τ EDM, d_τ, the BELLE Collaboration searched for CP-violation effects in the $e^+e^- \to \gamma^* \to \tau^+\tau^-$ process using triple momentum and spin correlations [23]. Through this reaction, they obtained the limits shown in Table I for the real and imaginary parts of the τ EDM. In the SM scenario, the theoretical predictions on the τ AMDM and EDM are: $a_\tau^{SM} = 117721(5) \times 10^{-8}$ [24–26] and $d_\tau^{SM} < 10^{-34}\, e\text{cm}$ [27–29],

respectively. These results are well below current experimental limits.

TABLE I: The best current experimental results for the electromagnetic dipole moments of the τ-lepton.

Collaboration	Best present experimental bounds on a_τ and d_τ	C.L.	Reference
DELPHI	$-0.052 < a_\tau < 0.013$	95 %	[22]
BELLE	$-2.2 < \mathrm{Re}(d_\tau(10^{-17}\, e\, cm)) < 4.5$	95 %	[23]
	$-2.5 < \mathrm{Im}(d_\tau(10^{-17}\, e\, cm)) < 0.08$	95 %	[23]

Another intrinsic property of the τ-lepton that has received attention in recent years due to important advances in the experimental domain consists of the weak dipole moments of the tau, which are associated with its interaction with the Z gauge boson. Both the AWMDM and the Weak Electric Dipole Moment (WEDM) of the τ-lepton, a_τ^W and d_τ^W, have been investigated with LEP data [30–32]. In Table II we show the current best experimental bounds on a_τ^W and d_τ^W. These limits are obtained through $\tau^+\tau^-$ production at LEP by the ALEPH Collaboration, corresponding to an integrated luminosity of 155 pb^{-1} [30]. On the theoretical side, the reached precisions in the AWMDM and WEDM of the tau-lepton are $a_\tau^{W-SM} = -(2.10 + 0.61\,\mathrm{i}) \times 10^{-6}$ [33] and $d_\tau^{W-SM} < 8 \times 10^{-34}$ $e$cm [34]. These values are well below the current experimental sensitivity. This opens the possibility of looking for deviations from the SM; therefore, studying extensions of the SM could generate significant contributions of new physics that are closer to the experimental bounds. With these motivations, we research on the electromagnetic and weak dipole moments of the tau-lepton in the context of the BLHM.

Based on everything already mentioned above, in this paper, we estimate the sensitivity bounds on the AMDM and AWMDM of the τ-lepton in the SM and BLHM scenario, and emphasis will be placed on the contributions generated by the particles predicted by the BLHM, as these quantify the new physics.

TABLE II: The best current experimental results for the weak dipole moments of the τ-lepton.

Collaboration	Best present experimental bounds on a_τ^W and d_τ^W	C.L.	Reference
ALEPH	$\lvert\mathrm{Re}(a_\tau^W)\rvert < 1.14 \times 10^{-3}$	95 %	[30]
	$\lvert\mathrm{Im}(a_\tau^W)\rvert < 2.65 \times 10^{-3}$	95 %	[30]
ALEPH	$\lvert\mathrm{Re}(d_\tau^W)\rvert < 0.50 \times 10^{-17}\, e\, cm$	95 %	[30]
	$\lvert\mathrm{Im}(d_\tau^W)\rvert < 1.1 \times 10^{-17}\, e\, cm$	95 %	[30]

The purpose of the BLHM is to solve the hierarchy problem without fine-tuning. This is achieved through the incorporation of one-loop corrections to the Higgs boson mass through heavy top-quarks partners and heavy gauge bosons. This extension of the SM predicts the existence of new physical scalar bosons neutral and charged $H_0, A_0, \phi^0, \eta^0, \sigma, H^\pm, \phi^\pm, \eta^\pm$, new heavy gauge bosons $Z', W'^\pm$ and new heavy quarks $B, T, T_5, T_6, T^{2/3}, T^{5/3}$. At the one-loop level, the AMDM a_τ and AWMDM a_τ^W of the τ-lepton are induced via the Feynman diagrams represented in Figs. 1 and 2, where S_i, $\Phi_i^\pm$ and H_i represent scalar bosons, V_i and $W_i^\pm$ gauge bosons, and l_i leptons. In the framework of the BLHM, new model contributions are those arising from the vertices of scalars bosons, vector bosons and vector-scalar bosons, that is to say, vertices of the form (see Figs. 1 and 2): $\gamma W'^+ W'^-$; $Z W'^+ W'^-$; $\gamma W_i^\pm \Phi_i^\pm$, $W_i^\pm = W^\pm, W'^\pm$, and $\Phi_i^\pm = \phi^\pm, \eta^\pm$; $Z W_i^\pm \Phi_i^\pm$; ZZH_0; $ZZ'H_i$, $H_i = h_0, H_0$; $H_0\tau\tau$; $\tau l_i S_i$, $S_i = H_0, A_0, \phi^0, \eta^0, \sigma, H^\pm, \phi^\pm, \eta^\pm$; $\tau l_i V_i$, $V_i = Z', W'^\pm$; $\gamma l_i \bar{l}_i$, and $Z l_i \bar{l}_i$, where $l_i = \tau, \nu_\tau$. With these vertices, we calculate the one-loop contributions to the AMDM and AWMDM of the τ-lepton and in several scenarios with $m_{A_0} = 1000$ GeV, $m_{\eta^0} = 100$ GeV, $\tan\beta = 3$, $f = [1000, 3000]$ GeV and $F = [3000, 6000]$ GeV.

The paper is structured as follows. In Section II, we give a brief review of the BLHM. In Section III, we present the predictions of the BLHM on the electromagnetic and weak dipole moments of the tau-lepton. In Section IV, we discuss the sensitivity bounds obtained on the AMDM and AWMDM of the τ-lepton. Finally, we present our conclusions in Section V. In Appendix A, we present the Feynman rules employed in the study of electromagnetic and weak dipole moments of the τ-lepton in the context of the BLHM. In Appendix B, we provide the one-loop level SM predictions on the AMDM and AWMDM of the tau-lepton.

II. THE BESTEST LITTLE HIGGS MODEL

Various extensions of the SM, such as Little Higgs Models (LHM) [35, 36], have been proposed to solve the problem of the mass hierarchy. This class of models employs a complex mechanism named collective symmetry breaking. The main idea is to represent the SM Higgs boson as a pseudo-Nambu-Goldstone boson of an approximate global symmetry that is spontaneously broken at a scale in the TeV range. In these models, the collective symmetry breaking mechanisms is implemented in the norm sector, fermion sector, and the Higgs sector, which predicts new particles within the mass range of a few TeV. These new particles play the role of partners of the top-quark, of the gauge bosons, and the Higgs boson, the effect of which is to generate radiative corrections for the mass of the Higgs boson and thus cancel the divergent corrections induced by SM particles. However, LHM [35–37] are already strongly constrained by electroweak precision data. These constraints typically require the new gauge bosons of LHM to be quite heavy [38, 39]. In most LHM, the top partners are heavier than the new gauge bosons, which can lead to significant fine-tuning in the Higgs potential [40].

An exciting and relatively recent model is the BLHM [41] overcomes these difficulties by including separate symmetry breaking scales at which the heavy gauge boson and top partners obtain their masses. This model generates heavy gauge boson partner masses above the excluded mass range and has light top partners below the upper bound from fine-tuning. The BLHM is based on two independent non-linear sigma models. With the first field Σ, the global symmetry $SO(6)_A \times SO(6)_B$ is broken to the diagonal group $SO(6)_V$ at the energy scale f, while with the second field Δ, the global symmetry $SU(2)_C \times SU(2)_D$ to the diagonal subgroup $SU(2)$ to the scale $F > f$. In the first stage are generated 15 pseudo-Nambu-Goldstone bosons that are parameterized as

$$\Sigma = e^{i\Pi/f} e^{2i\Pi_h/f} e^{i\Pi/f}, \tag{1}$$

where Π and Π_h are complex and antisymmetric matrices given in Ref. [41]. Regarding the second stage of spontaneous symmetry-breaking, the pseudo-Nambu-Goldstone bosons of the field Δ are parameterized as follows

$$\Delta = F e^{2i\Pi_d/F}, \quad \Pi_d = \chi_a \frac{\tau^a}{2} \quad (a = 1, 2, 3), \tag{2}$$

χ_a represents the Nambu-Goldstone fields and the τ_a correspond to the Pauli matrices [41], which are the generators of the SU(2) group.

A. The scalar sector

The BLHM Higgs fields, h_1 and h_2, form the Higgs potential that undergoes spontaneous symmetry breaking [41–43]:

$$V_{Higgs} = \frac{1}{2}m_1^2 h_1^T h_1 + \frac{1}{2}m_2^2 h_2^T h_2 - B_\mu h_1^T h_2 + \frac{\lambda_0}{2}(h_1^T h_2)^2. \tag{3}$$

The potential reaches a minimum when $m_1, m_2 > 0$, while to break the electroweak symmetry requires $B_\mu > m_1 m_2$. The symmetry-breaking mechanism is implemented in the BLHM when the Higgs doublets acquire their vacuum expectation values (VEVs), $\langle h_1 \rangle^T = (v_1, 0, 0, 0)$ and $\langle h_2 \rangle^T = (v_2, 0, 0, 0)$. By demanding that these VEVs minimize the Higgs potential of Eq. (3), the following relations are obtained

$$v_1^2 = \frac{1}{\lambda_0}\frac{m_2}{m_1}(B_\mu - m_1 m_2), \tag{4}$$

$$v_2^2 = \frac{1}{\lambda_0}\frac{m_1}{m_2}(B_\mu - m_1 m_2). \tag{5}$$

These parameters can be expressed as follows

$$v^2 \equiv v_1^2 + v_2^2 = \frac{1}{\lambda_0}\left(\frac{m_1^2 + m_2^2}{m_1 m_2}\right)(B_\mu - m_1 m_2) \simeq (246 \ \ \text{GeV})^2, \tag{6}$$

$$\tan\beta = \frac{v_1}{v_2} = \frac{m_2}{m_1}. \tag{7}$$

From the diagonalization of the mass matrix for the scalar sector, three non-physical fields G_0 and $G^\pm$, two physical scalar fields $H^\pm$ and three neutral physical scalar fields h_0, H_0 and A_0 are generated [42, 44]. The lightest state, h_0, is identified as the scalar boson of the SM. The masses of these fields are given as

$$m_{G_0} = m_{G^\pm} = 0, \tag{8}$$

$$m_{A_0}^2 = m_{H^\pm}^2 = m_1^2 + m_2^2, \tag{9}$$

$$m^2_{H_0} = \frac{B_\mu}{\sin 2\beta} + \sqrt{\frac{B^2_\mu}{\sin^2 2\beta} - 2\lambda_0 B_\mu v^2 \sin 2\beta + \lambda_0^2 v^4 \sin^2 2\beta}. \quad (10)$$

The four parameters present in the Higgs potential m_1, m_2, B_μ and λ_0 can be replaced by another more phenomenologically accessible set. That is, the masses of the states h_0 and A_0, the angle β and the VEV v [42]:

$$B_\mu = \frac{1}{2}(\lambda_0 v^2 + m^2_{A_0}) \sin 2\beta, \quad (11)$$

$$\lambda_0 = \frac{m^2_{h_0}}{v^2}\Big(\frac{m^2_{h_0} - m^2_{A_0}}{m^2_{h_0} - m^2_{A_0} \sin^2 2\beta}\Big), \quad (12)$$

$$\tan\alpha = \frac{B_\mu \cot 2\beta + \sqrt{(B^2_\mu/\sin^2 2\beta) - 2\lambda_0 B_\mu v^2 \sin 2\beta + \lambda_0^2 v^4 \sin^2 2\beta}}{B_\mu - \lambda_0 v^2 \sin 2\beta}, \quad (13)$$

$$m^2_{H_0} = \frac{B_\mu}{\sin 2\beta} + \sqrt{\frac{B^2_\mu}{\sin^2 2\beta} - 2\lambda_0 B_\mu v^2 \sin 2\beta + \lambda_0^2 v^4 \sin^2 2\beta}, \quad (14)$$

$$m^2_\sigma = (\lambda_{56} + \lambda_{65}) f^2 = 2\lambda_0 f^2 \mathrm{K}_\sigma. \quad (15)$$

The variables λ_{56} and λ_{65} in Eq. (15) represent the coefficients of the quartic potential defined in [41], both variables take values different from zero to achieve the collective breaking of the symmetry and generate a quartic coupling of the Higgs boson [41, 42]. The BLHM also contains scalar triplet fields that get a contribution to their mass from the explicit symmetry breaking terms in the model, as defined in Ref. [41], that depends on the parameter m_4.

$$m^2_{\phi^0} = \frac{16}{3} F^2 \frac{3 g_A^2 g_B^2}{32\pi^2} \log\left(\frac{\Lambda^2}{m^2_{W'^\pm}}\right) + m_4^2 \frac{f^4 + F^4}{F^2(f^2 + F^2)}, \quad (16)$$

$$m^2_{\phi^\pm} = \frac{16}{3} F^2 \frac{3 g_A^2 g_B^2}{32\pi^2} \log\left(\frac{\Lambda^2}{m^2_{W'^\pm}}\right) + m_4^2 \frac{f^4 + f^2 F^2 + F^4}{F^2(f^2 + F^2)}, \quad (17)$$

$$m^2_{\eta^\pm} = m_4^2 + \frac{3 f^2 g_Y^2}{64\pi^2} \frac{\Lambda^2}{F^2}, \quad (18)$$

$$m^2_{\eta^0} = m_4^2. \quad (19)$$

B. The gauge sector

In the BLHM, the new gauge bosons develop masses proportional to $\sqrt{f^2 + F^2} \sim F$. This makes the masses of the gauge bosons large relative to other particles that have masses proportional to f. The kinetic terms of the gauge fields in the BLHM are given as follows:

$$\mathcal{L} = \frac{f^2}{8}\mathrm{Tr}(D_\mu \Sigma^\dagger D^\mu \Sigma) + \frac{F^2}{4}\mathrm{Tr}(D_\mu \Delta^\dagger D^\mu \Delta), \tag{20}$$

where

$$D_\mu \Sigma = \partial_\mu \Sigma + i g_A A^a_{1\mu} T^a_L \Sigma - i g_B \Sigma A^a_{2\mu} T^a_L + i g_Y B^3_\mu (T^3_R \Sigma - \Sigma T^3_R), \tag{21}$$

$$D_\mu \Delta = \partial_\mu \Delta + i g_A A^a_{1\mu} \frac{\tau^a}{2} \Delta - i g_B \Delta A^a_{2\mu} \frac{\tau^a}{2}. \tag{22}$$

T^a_L are the generators of the group $SO(6)_A$ corresponding to the subgroup $SU(2)_{LA}$, while T^3_R represents the third component of the $SO(6)_B$ generators corresponding to the $SU(2)_{LB}$ subgroup, these matrices are provided in [41]. g_A and $A^a_{1\mu}$ denote the gauge coupling and field associated with the gauge bosons of $SU(2)_{LA}$. g_B and $A^a_{2\mu}$ represent the gauge coupling and the field associated with $SU(2)_{LB}$, while g_Y and B^3_μ denote the hypercharge and the field. When Σ and Δ get their VEVs, the gauge fields $A^a_{1\mu}$ and $A^a_{2\mu}$ are mixed to form a massless triplet $A^a_{0\mu}$ and a massive triplet $A^a_{H\mu}$,

$$A^a_{0\mu} = \cos\theta_g A^a_{1\mu} + \sin\theta_g A^a_{2\mu}, \quad A^a_{H\mu} = \sin\theta_g A^a_{1\mu} - \cos\theta_g A^a_{2\mu}, \tag{23}$$

with the mixing angles

$$s_g \equiv \sin\theta_g = \frac{g_A}{\sqrt{g_A^2 + g_B^2}}, \quad c_g \equiv \cos\theta_g = \frac{g_B}{\sqrt{g_A^2 + g_B^2}}, \tag{24}$$

which are related to the electroweak gauge coupling g through

$$\frac{1}{g^2} = \frac{1}{g_A^2} + \frac{1}{g_B^2}. \tag{25}$$

After breaking the electroweak symmetry, when the Higgs doublets, h_1 and h_2 acquire their VEVs, the masses of the gauge bosons of the BLHM are generated. In terms of the model parameters, the masses are given by

$$m^2_\gamma = 0 \ , \tag{26}$$

$$m^2_Z = \frac{1}{4}\left(g^2 + g_Y^2\right) v^2 \left(1 - \frac{v^2}{12 f^2}\left(2 + \frac{3 f^2}{f^2 + F^2}\left(s_g^2 - c_g^2\right)^2\right)\right), \tag{27}$$

$$m^2_{W^\pm} = \frac{1}{4} g^2 v^2 \left(1 - \frac{v^2}{12 f^2}\left(2 + \frac{3 f^2}{f^2 + F^2}\left(s_g^2 - c_g^2\right)^2\right)\right), \tag{28}$$

$$m^2_{Z'} = m^2_{W'^{\pm}} + \frac{g^2 s_W^2 v^4}{16 c_W^2 (f^2+F^2)} \left(s_g^2 - c_g^2\right)^2, \tag{29}$$

$$m^2_{W'^{\pm}} = \frac{g^2}{4 c_g^2 s_g^2}\left(f^2+F^2\right) - m^2_{W^{\pm}}. \tag{30}$$

The weak mixing angle is defined as

$$s_W \equiv \sin\theta_W = \frac{g_Y}{\sqrt{g^2+g_Y^2}}, \tag{31}$$

$$c_W \equiv \cos\theta_W = \frac{g}{\sqrt{g^2+g_Y^2}}. \tag{32}$$

C. The Yang-Mills sector

The gauge boson self-interactions arise from the following Lagrangian terms:

$$\mathcal{L} = F_{1\mu\nu}F_1^{\mu\nu} + F_{2\mu\nu}F_2^{\mu\nu}, \tag{33}$$

where $F_{1,2}^{\mu\nu}$ are given by:

$$F_1^{\mu\nu} = \partial^\mu A_1^{\alpha\nu} - \partial^\nu A_1^{\alpha\mu} + g_A \sum_b \sum_c \epsilon^{abc} A_1^{b\mu} A_1^{c\nu}, \tag{34}$$

$$F_2^{\mu\nu} = \partial^\mu A_2^{\alpha\nu} - \partial^\nu A_2^{\alpha\mu} + g_B \sum_b \sum_c \epsilon^{abc} A_2^{b\mu} A_2^{c\nu}. \tag{35}$$

In these equations, the indices a, b and c run over the three gauge fields [45]; ϵ^{abc} is the anti-symmetric tensor.

D. The fermion sector

To construct the Yukawa interactions in the BLHM, the fermions must be transformed under the group $SO(6)_A$ or $SO(6)_B$. In this model, the fermion sector is divided into two parts. First, the sector of massive fermions is represented by Eq. (36). This sector includes the top and bottom quarks of the SM and a series of new heavy quarks arranged in four multiplets, Q, and Q' which transform under $SO(6)_A$, while U^c and $U_5'^c$ are transformed under the group $SO(6)_B$. Second, the sector of light fermions contained in Eq. (37), in this

expression, all the interactions of the remaining fermions of the SM with the exotic particles of the BLHM are generated.

For massive fermions, the Lagrangian that describes them is given by [41]

$$\mathcal{L}_t = y_1 f Q^T S\Sigma S U^c + y_2 f Q'^T \Sigma U^c + y_3 f Q^T \Sigma U_5'^c + y_b f q_3^T(-2iT_R^2\Sigma)U_b^c + h.c., \tag{36}$$

where $S = \text{diag}(1,1,1,1,-1,-1)$. The explicit representation of the multiplets involved in Eq. (36) is provided in Refs. [41, 44]. For simplicity, the Yukawa couplings are assumed to be real $y_1, y_2, y_3 \in R$.

For light fermions the corresponding Lagrangian is [41, 44, 45]

$$\mathcal{L}_{light} = \sum_{i=1,2} y_u f q_i^T \Sigma u_i^c + \sum_{i=1,2} y_d f q_i^T(-2iT_R^2\Sigma)d_i^c + \sum_{i=1,2,3} y_e f l_i^T(-2iT_R^2\Sigma)e_i^c + h.c. \tag{37}$$

E. The currents sector

The Lagrangian that describes the interactions of fermions with the gauge bosons is [41, 44]

$$\begin{aligned}\mathcal{L} \;=\; & \bar{Q}\bar{\tau}^\mu D_\mu Q + \bar{Q}'\bar{\tau}^\mu D_\mu Q' - U^{c\dagger}\tau^\mu D_\mu U^c - U'^{c\dagger}\tau^\mu D_\mu U'^c - U_b^{c\dagger}\tau^\mu D_\mu U_b^c + \sum_{i=1,2} q_i^\dagger \tau^\mu D_\mu q_i \\ & + \sum_{i=1,2,3} l_i^\dagger \tau^\mu D_\mu l_i - \sum_{i=1,2,3} e_i^{c\dagger}\tau^\mu D_\mu e_i^c - \sum_{i=1,2} u_i^{c\dagger}\tau^\mu D_\mu u_i^c - \sum_{i=1,2} d_i^{c\dagger}\tau^\mu D_\mu d_i^c,\end{aligned} \tag{38}$$

where τ^μ and $\bar{\tau}^\mu$ are defined according to [46]. On the other hand, the respective covariant derivatives are provided in Refs. [44, 45].

III. ELECTROMAGNETIC AND WEAK DIPOLE MOMENTS OF THE TAU-LEPTON IN THE BLHM

The electroweak properties of fermions are characterized by physical magnitudes called form factors. These measure properties such as the electric charge, the AMDM, the EDM, the AWMDM, the WEDM, and others. Some of these quantities are already present in classical theory, while others arise for the first time as a quantum fluctuation of one-loop or higher orders. In quantum field theory, the electromagnetic and weak properties of fermions arise through their interaction with the gauge boson V, $V = \gamma, Z$. The most general Lorentz-invariant vertex function describing the interaction of a gauge boson with two fermions can be

written in terms of ten form factors [47, 48], which are functions of the kinematic invariants. In the low energy limit, these correspond to couplings that multiply dimension-four or-five operators in an effective Lagrangian and may be complex. If the gauge boson V is on-shell, or if V couples to effectively massless fermions, the number of independent form factors is reduced to eight. In addition, if the fermions are on-shell, the number is further reduced to four. In this way, the $V\bar{f}f$ vertex function can be written in the form

$$ie\bar{u}(p')\Gamma^{\mu}_{V\bar{f}f}u(p) = ie\bar{u}(p')\{\gamma^{\mu}\left[F_V^V(q^2) - F_A^V(q^2)\gamma^5\right] + i\sigma^{\mu\nu}q_{\nu}\left[F_M^V(q^2) - iF_E^V(q^2)\gamma^5\right]\}u(p), \quad (39)$$

where e is the proton charge and $q = p' - p$ the V gauge boson transferred four-momentum. The terms $F_V^V(0)$ and $F_A^V(0)$ in the low energy limit are the $V\bar{f}f$ vector and axial-vector form factors in the SM, while $F_M^V(q^2)$ and $F_E^V(q^2)$ are associated with the form factors of the electromagnetic or weak dipole moments. The latter arise at the loop level and are a valuable tool to study the effects of new physics indirectly, through virtual corrections of new particles predicted by extensions of the SM. The AWMDM and WEDM are given by $a_f^W = -2m_f F_M^Z(q^2 = m_Z^2)$ and $d_f^W = -eF_E^Z(q^2 = m_Z^2)$, whereas the electromagnetic properties, a_f and d_f, are defined by analogue expressions but with the replacement $q^2 = 0$.

A. The AMDM and AWMDM of the tau-lepton at the BLHM

In this subsection, we are interested in the contributions generated by the new BLHM particles to the electromagnetic and weak dipole moments of the tau-lepton. At the one-loop level, the τ EDM and WEDM are absent, so they do not receive contributions of the radiative corrections. However, the τ AMDM and AWMDM are induced by scalar bosons, vector bosons and, leptons via the Feynman diagrams depicted in Figs. 1 and 2. In these figures, S_i and $\Phi_i^{\pm}$ represent the new scalars $A_0, H_0, H^{\pm}, \eta^0, \phi^0, \sigma, \eta^{\pm}, \phi^{\pm}$; V_i stands for the new gauge bosons $Z', W'^{\pm}$, and $W_i^{\pm}$ the gauge bosons $W^{\pm}, W'^{\pm}$; and finally, l_i denotes the leptons τ, ν_{τ}. To obtain the amplitude of each contribution, we use the Feynman rules provided in Appendix A [49]. We used the unitary gauge for our calculations and implemented the Passarino-Veltman reduction scheme to solve the loop integrals involved in the amplitudes. Such amplitudes are also gauge independent since the V gauge boson is in on-shell, as well

as the tau-lepton pair. It is worth mentioning that the contributions for the AMDM and AWMDM of the τ-lepton are free of divergences.

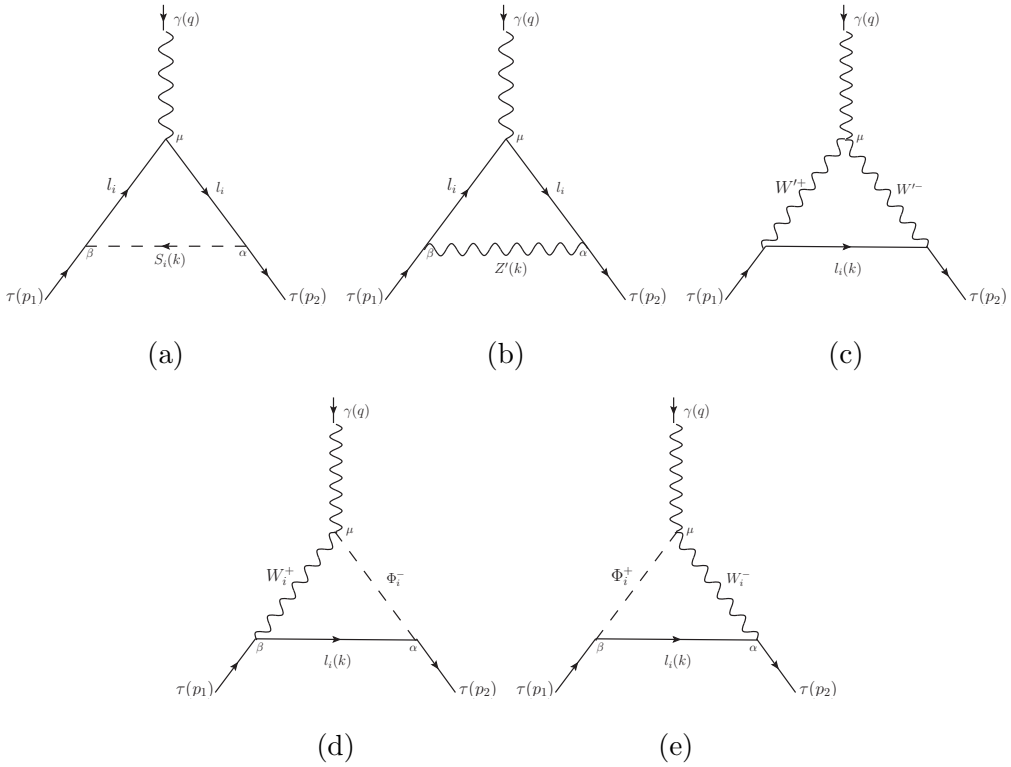

FIG. 1: Generic Feynman diagrams that contribute to the AMDM of the tau-lepton, $l_i \equiv \tau, \nu_\tau$. a) Scalar contributions, $S_i \equiv \sigma, A_0, H_0, \eta^0, \phi^0$. b) and c) Vector contributions, $V_i \equiv Z', W'^{\pm}$. d) and e) Scalar-vector contributions, $W_i^{\pm} = W^{\pm}, W'^{\pm}$, and $\Phi_i^{\pm} = \phi^{\pm}, \eta^{\pm}$.

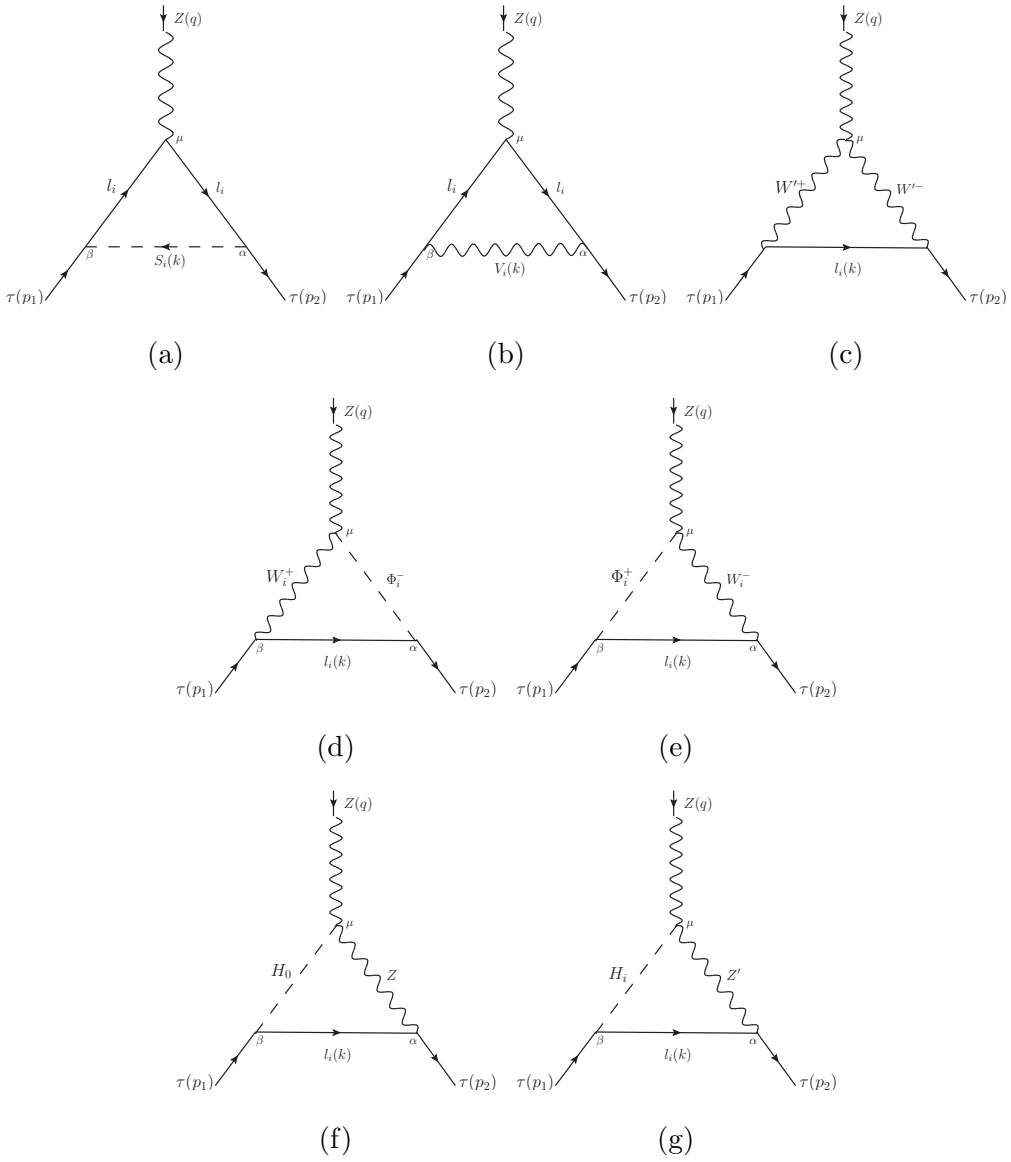

FIG. 2: Generic Feynman diagrams that contribute to the AWMDM of the tau-lepton, $l_i \equiv \tau, \nu_\tau$. a) Scalar contributions, $S_i \equiv A_0, H_0, H^\pm, \eta^0, \phi^0, \sigma, \eta^\pm, \phi^\pm$. b) and c) Vector contributions, $V_i \equiv Z', W'^\pm$. d), e), f) and g) Scalar-vector contributions, $W_i^\pm = W^\pm, W'^\pm$, $\Phi_i^\pm = \phi^\pm, \eta^\pm$, and $H_i = h_0, H_0$.

According to Figs. 1 and 2, all possible amplitudes contributing to the $F_M^\gamma(q^2)$ or $F_M^Z(q^2)$ form factors can be classified in terms of the six classes of triangle diagrams. Each category can be written in the following compact notation

$$
\begin{aligned}
\mathcal{M}_\tau^\mu(S_i l_i l_i) &= C^2_{\tau l_i S_i}\int\frac{d^4k}{(2\pi)^4}\bar{u}(p_2)\left[i\frac{\not{k}+\not{p}_2+m_{l_i}}{(k+p_2)^2-m^2_{l_i}}\right]\left(\gamma^\mu(F_{V_i}+F_{A_i}\gamma^5)\right)\\
&\times\left[i\frac{\not{k}+\not{p}_1+m_{l_i}}{(k+p_1)^2-m^2_{l_i}}\right]u(p_1)\left(\frac{i}{k^2-m^2_{S_i}}\right), \qquad (40)\\
\mathcal{M}_\tau^\mu(V_i l_i l_i) &= \int\frac{d^4k}{(2\pi)^4}\bar{u}(p_2)\left(C^*_{\tau l_i V_i}\gamma^\alpha P_L\right)\left[i\frac{\not{k}+\not{p}_2+m_{l_i}}{(k+p_2)^2-m^2_{l_i}}\right]\left(\gamma^\mu(F_{V_i}+F_{A_i}\gamma^5)\right)\\
&\times\left[i\frac{\not{k}+\not{p}_1+m_{l_i}}{(k+p_1)^2-m^2_{l_i}}\right]\left(C_{\tau l_i V_i}\gamma^\beta P_L\right)u(p_1)\\
&\times\left[\frac{i}{k^2-m^2_{V_i}}\left(-g_{\alpha\beta}+\frac{k_\alpha k_\beta}{m^2_{V_i}}\right)\right], \qquad (41)\\
\mathcal{M}_\tau^\mu(W'^+W'^- l_i) &= \int\frac{d^4k}{(2\pi)^4}\bar{u}(p_2)\left(C^*_{\tau l_i W'}\gamma^\nu P_L\right)\left[i\frac{\not{k}}{k^2}\right]\left(C_{\tau l_i W'}\gamma^\lambda P_L\right)u(p_1)\\
&\times\left[\frac{i}{(k-p_2)^2-m^2_{W'}}\left(-g_{\alpha\nu}+\frac{(k-p_2)_\alpha(k-p_2)_\nu}{m^2_{W'}}\right)\right]A^{\alpha\mu\beta}_{VW'W'}\\
&\times\left[\frac{i}{(k-p_1)^2-m^2_{W'}}\left(-g_{\beta\lambda}+\frac{(k-p_1)_\beta(k-p_1)_\lambda}{m^2_{W'}}\right)\right], \qquad (42)\\
\mathcal{M}_\tau^\mu(\Phi_i^- W_i^+ l_i) &= \int\frac{d^4k}{(2\pi)^4}\bar{u}(p_2)\left(C_{\tau l_i\Phi_i^-}\right)\left[i\frac{\not{k}}{k^2}\right]\left(C_{\tau l_i W_i^+}\gamma^\beta P_L\right)u(p_1)\\
&\times\left[\frac{i}{(k-p_2)^2-m^2_{\Phi_i^-}}\right]\left(C_{W_i^+V\Phi_i^-}\,g^{\mu\nu}\right)\\
&\times\left[\frac{i}{(k-p_1)^2-m^2_{W_i^+}}\left(-g_{\beta\nu}+\frac{(k-p_1)_\beta(k-p_1)_\nu}{m^2_{W_i^+}}\right)\right], \qquad (43)\\
\mathcal{M}_\tau^\mu(W_i^-\Phi_i^+ l_i) &= \int\frac{d^4k}{(2\pi)^4}\bar{u}(p_2)\left(C_{\tau l_i W_i^-}\gamma^\alpha P_L\right)\left[i\frac{\not{k}}{k^2}\right]\left(C_{\tau l_i\Phi_i^+}\right)u(p_1)\\
&\times\left[\frac{i}{(k-p_2)^2-m^2_{W_i^+}}\left(-g_{\alpha\nu}+\frac{(k-p_2)_\alpha(k-p_2)_\nu}{m^2_{W_i^-}}\right)\right]\\
&\times\left(C_{W_i^-V\Phi_i^+}\,g^{\mu\nu}\right)\left[\frac{i}{(k-p_1)^2-m^2_{\Phi_i^+}}\right], \qquad (44)\\
\mathcal{M}_\tau^\mu(\mathtt{Z}H_i l_i) &= \int\frac{d^4k}{(2\pi)^4}\bar{u}(p_2)\left(\gamma^\alpha(F_{V_i}+F_{A_i}\gamma^5)\right)\left[i\frac{\not{k}+m_\tau}{k^2-m^2_\tau}\right](C_{\tau l_i H_i})\,u(p_1)\\
&\times\left[\frac{i}{(k-p_2)^2-m^2_{\mathtt{Z}}}\left(-g_{\alpha\nu}+\frac{(k-p_2)_\alpha(k-p_2)_\nu}{m^2_{\mathtt{Z}}}\right)\right](C_{H_i Z\mathtt{Z}}\,g^{\mu\nu})\\
&\times\left[\frac{i}{(k-p_1)^2-m^2_{H_i}}\right], \qquad (45)
\end{aligned}
$$

where F_{V_i} and F_{A_i} denote the form factors of the vector and axial-vector. On the other hand, $\mathtt{Z}=Z,Z'$, while C (or C^*) denotes the coupling constants of the corresponding vertices. The

tensor $A^{\alpha\mu\beta}_{VW'W'}$ is provided in Table IX of Appendix A. From these amplitudes, we obtain the new physics contributions induced by the scalar and vector bosons, particles of the BLHM. The effects of the new physics are determined in the following way

$$a_\tau \equiv a_\tau^{BLHM} = [a_\tau]^{S_i} + [a_\tau]^{V_i} + [a_\tau]^{S_i - V_i}, \tag{46}$$

$$a_\tau^W \equiv a_\tau^{W-BLHM} = [a_\tau^W]^{S_i} + [a_\tau^W]^{V_i} + [a_\tau^W]^{S_i - V_i}. \tag{47}$$

We also consider the total contributions, that is, which result from the sum of the contributions of the SM (see Appendix B) and BLHM.

$$\alpha_\tau = a_\tau^{SM} + a_\tau^{BLHM}, \tag{48}$$

$$\alpha_\tau^W = a_\tau^{W-SM} + a_\tau^{W-BLHM}. \tag{49}$$

IV. NUMERICAL RESULTS

For our numerical analysis of the electromagnetic and weak properties of the tau-lepton in the context of the SM and BLHM, we briefly review the free parameters of the BLHM. Subsequently, we discuss the numerical contributions generated for the AMDM and AWMDM of the τ-lepton in each study scenario.

A. Parameters space of the BLHM

We consider the following BLHM input parameters: m_{A_0}, m_{η_0}, $\tan\beta$, $\tan\theta_g$, f and F.

The pseudoscalar mass A_0: This parameter is fixed around 1000 GeV, our choice is consistent with the current search results for new scalar bosons [50]. Data recorded by the ATLAS experiment at the LHC, corresponding to an integrated luminosity of 139 fb^{-1} from proton-proton collisions at a center-of-mass energy 13 TeV, were used to search for a heavy Higgs boson, A_0, decaying into ZH, where H denotes another heavy Higgs boson with mass $m_H > 125$ GeV.

The scalar mass η_0: In the BLHM scenario, the free parameters $m_{4,5,6}$ [41] are introduced to break all the axial symmetries in the Higgs potential, giving positive masses to all scalars.

Specifically, the η_0 scalar receives a mass equal to $m_4 = m_{\eta_0} = 100$ GeV, according to the BLHM, and the restriction $m_4 \gtrsim 10$ GeV must be considered [41].

The ratio of the VEVs of the two Higgs doublets, $\tan\beta$: Several theoretical constraints can be applied to this parameter, primarily due to perturbativity requirements. Two constraints limit the value of $\tan\beta$, the first of which is the requirement that $\lambda_0 < 4\pi$, leading to an upper bound according to Eq. (50). A lower bound also exits and is set by examining the radiatively induced contributions to m_1 and m_2 in the model, which suggests that $\tan\beta > 1$ [41].

$$1 < \tan\beta < \sqrt{\frac{2 + 2\sqrt{(1 - \frac{m_{h_0}^2}{m_{A_0}^2})(1 - \frac{m_{h_0}^2}{4\pi v^2})}}{\frac{m_{h_0}^2}{m_{A_0}^2}(1 + \frac{m_{A_0}^2 - m_{h_0}^2}{4\pi v^2})}} - 1. \tag{50}$$

From this inequality, we can find the range of allowed values for the parameter $\tan\beta$. In particular, for $m_{A_0} = 1000$ GeV, it is obtained that $1 < \tan\beta < 10.45$.

The mixing angle θ_g: The gauge couplings g_A and g_B, associated with the $SU(2)_{LA}$ and $SU(2)_{LB}$ gauge bosons, can be parametrized in a more phenomenological fashion in terms of a mixing angle θ_g and the $SU(2)_L$ gauge coupling: $\tan\theta_g = g_A/g_B$ and $g = g_A g_B/\sqrt{g_A^2 + g_B^2}$. For simplicity, it is assumed that $\tan\theta_g = 1$ [44], which implies that the gauge couplings g_A and g_B are equal. The $g_{A,B}$ values are generated using the restriction $g = 0.6525$.

Symmetry breaking scale f: The BLHM features a global $SO(6)_A \times SO(6)_B$ symmetry that is broken to a diagonal $SO(6)_V$ at a scale $f \sim \mathcal{O}(\text{TeV})$ when a nonlinear sigma field, $\sum$, develop a VEV. Bounds on the f scale arise when $\tan\beta$ limits, fine-tuning constraints on the heavy quark masses, and experimental restrictions from producing of heavy quarks are considered. Refs. [42] and [51] establish that $f \in (700, 3000)$ GeV.

Symmetry breaking scale F: A second global symmetry of the $SU(2)_C \times SU(2)_D$ form is also present in the BLHM, and is broken to a diagonal $SU(2)$ at a scale $F > f$ when a second nonlinear sigma field, Δ, develops a VEV. Due to the characteristics of the BLHM, the energy scale F acquires sufficiently large values compared to the f scale. The purpose is to ensure that the new gauge bosons are much heavier than the exotic quarks. In this way, $F \in [3000, 6000]$ GeV [41, 42].

To predict the estimates of the AMDM and AWMDM of the tau-lepton, in Table III, we

summarize the values used for the parameters involved in our analysis.

TABLE III: Values assigned to the free parameters involved in our numerical analysis in the context of the BLHM.

Parameter	**Value**
m_{A_0}	1000 GeV
m_{η^0}	100 GeV
$\tan\beta$	3
$\tan\theta_g$	1
f	$[1000, 3000]$ GeV
F	$[3000, 6000]$ GeV

B. AMDM of the tau-lepton at the BLHM

At the one-loop level, the electromagnetic properties of the tau-lepton are induced by the scalar and vector bosons of the BLHM via the Feynman diagrams of Fig. 1. The contributions generated by these diagrams are classified into three types for analysis: scalar, vector, and scalar-vector. Below, we focus on the potential effects of the new particles that contribute to the AMDM of tau-lepton, as they could generate a significant enhancement in the value of a_τ ($a_\tau \equiv a_\tau^{BLHM}$) compared to the SM prediction a_τ^{SM}. In the BLHM, as in the SM, the τ EDM is multiloop suppressed. Therefore, in this subsection, we report only the values of a_τ.

For this purpose, we start by solving the amplitudes generated by Eqs. (40)-(44), the method we use to solve is the Passarino-Veltman reduction scheme. As indicated above, Table III assigns values to the free parameters involved in our numerical analysis. The parameter $\tan\theta_g = g_A/g_B$ is of particular interest since in this paper, as in Ref. [44], it is assumed for simplicity that $\tan\theta_g = 1$ which implies that the gauge couplings g_A and g_B are equal. Another possible study scenario it is for $\tan\theta_g \neq 1$ ($\sin\theta_g \neq \cos\theta_g$). In this case, we can predict that the values for a_τ and a_τ^W do not change significantly in this new scenario. As will be shown later, the reason for this is that the Feynman rules for vertices that involve diagrams that provide the largest contributions (see Figs. 1(a) and 2(a)), that is,

the terms that contain $\sin\theta_g$ and $\cos\theta_g$ are inversely proportional to (f^2+F^2) (see Table IX in Appendix A), and therefore suppress these additional contributions since $f \in [1000, 3000]$ GeV and $F \in [3000, 6000]$ GeV. When $\tan\theta_g = 1$, the Feynman rules for the $A_\gamma W^+\phi^-$ and $A_\gamma W^+\eta^-$ vertices, as well as their respective Hermitian conjugates, are canceled (see Table X in Appendix A). Thus, they lead to the non-contribution of specific Feynman diagrams shown in Figs. 1(d) and 1(e).

After solving for the amplitudes, we extract the form factors proportional to the $\sigma^{\mu\nu}q_\nu$ tensor, these form factors contain in coded away the $[a_\tau]^{S_i}$, $[a_\tau]^{V_i}$ and $[a_\tau]^{S_i-V_i}$. Concerning $[a_\tau]^{S_i-V_i}$ that represents the scalar-vector contributions to the AMDM of the τ-lepton, its corresponding form factors turn out to be zero. Therefore, $[a_\tau]^{S_i-V_i}$ has no effect on a_τ. The only non-zero contributions to the AMDM a_τ of the tau-lepton arise due to the scalar contributions and vector contributions shown in Figs. 1(a) and 1(b)-1(c), respectively.

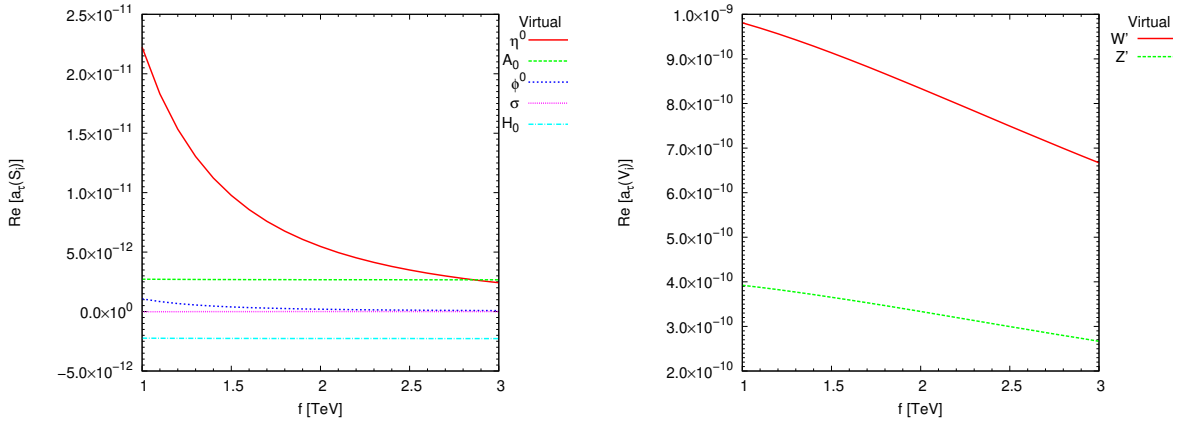

(a) (b)

FIG. 3: a) Individual scalar contributions to Re(a_τ). b) Individual vector contributions to Re(a_τ). The plots are obtained with the fixed value of $F = 4000$ GeV. The values provided in Table III are used for the remaining model parameters.

In Fig. 3, we show the partial contributions to a_τ due to the different particles involved, and these individual contributions are classified in $a_\tau(S_i)$ and $a_\tau(V_i)$, depend on the energy scale f and generate purely real values. Specifically, Fig. 3(a) shows the curves of the contributions generated by the scalars η^0, A_0, ϕ^0, σ and H_0. In this figure, we can appreciate that the scalar η^0 provides the largest positive contribution with Re$[a_\tau(\eta^0)]$ $= [2.22 \times 10^{-11}, 2.43 \times 10^{-12}]$ while the smallest negative contribution is given by the H_0

scalar with $\mathrm{Re}[a_\tau(H_0)] = -[2.24, 2.27] \times 10^{-12}$. The remaining scalars generate suppressed contributions, one or more orders of magnitude smaller compared to the main contribution $\mathrm{Re}[a_\tau(\eta^0)]$: $\mathrm{Re}[a_\tau(A_0)] = [2.72, 2.67] \times 10^{-12}$, $\mathrm{Re}[a_\tau(\phi^0)] = [1.07 \times 10^{-12}, 7.82 \times 10^{-14}]$ and $\mathrm{Re}[a_\tau(\sigma)] = [2.09 \times 10^{-14}, 2.96 \times 10^{-16}]$. On the other hand, the vector contributions arise from the gauge bosons W' and Z' (see Fig. 3(b)). So for the range of analysis set for the symmetry breaking scale f, the contribution of the gauge bosons $W'^{\pm}$ and Z' are $\mathrm{Re}[a_\tau(W'^{\pm})] = [9.81, 6.67] \times 10^{-10}$ and $\mathrm{Re}[a_\tau(Z')] = [3.92, 2.67] \times 10^{-10}$, respectively. According to Figs. 3(a) and 3(b), we observe that the main partial contribution to $\mathrm{Re}[a_\tau]$ is generated by the $W'^{\pm}$ gauge boson. We also notice that as the energy scale f takes values closer to 3000 GeV, the values of $\mathrm{Re}[a_\tau]$ become smaller and smaller. In Table IV we show the magnitudes of all partial contributions to a_τ that correspond to the virtual particles circulating in the $\gamma\tau^+\tau^-$ vertex loop.

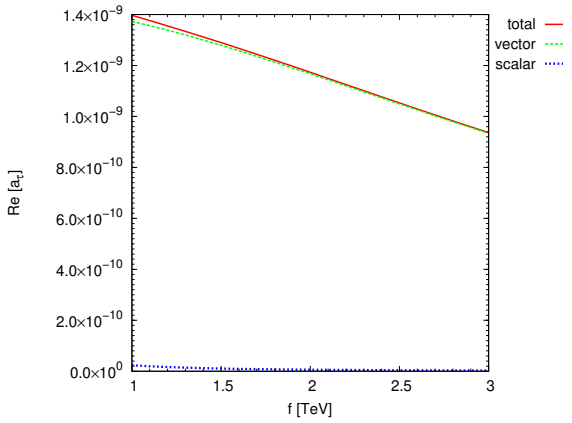

FIG. 4: Scalar, vector and total contributions to $\mathrm{Re}(a_\tau)$. The plot is obtained with the fixed value of $F = 4000$ GeV. The values provided in Table III are used for the remaining model parameters.

In Fig. 4, we also describe the behavior of $\mathrm{Re}[a_\tau(\mathrm{scalar})]$ and $\mathrm{Re}[a_\tau(\mathrm{vector})]$, as well as the total of these two contributions. $\mathrm{Re}[a_\tau(\mathrm{scalar})]$ and $\mathrm{Re}[a_\tau(\mathrm{vector})]$ stand for the sum of all individual contributions to $\mathrm{Re}[a_\tau]$ due to the scalar and vector bosons, respectively. Note that the magnitude of the vector contribution dominates concerning the scalar contribution so that the total contribution receives significant contributions from the vector sector. The numerical estimates obtained for the three sectors are $\mathrm{Re}[a_\tau(\mathrm{vector})] = [1.37 \times 10^{-9}, 9.34 \times 10^{-10}]$, $\mathrm{Re}[a_\tau(\mathrm{scalar})] = [2.38 \times 10^{-11}, 2.90 \times 10^{-12}]$ and $\mathrm{Re}[a_\tau(\mathrm{total})] = [1.40 \times 10^{-9}, 9.37 \times$

$10^{-10}]$ for $f = [1000, 3000]$ GeV. According to these numerical data, we find that effectively the vector and total contribution acquire values of the same order of magnitude, which does not occur with the scalar contribution, which generates slightly small contributions, thus interfering very weakly with the total contribution.

Until now, the sensitivity of the total AMDM of the tau-lepton has been measured by varying the first symmetry breaking scale f. However, it also depends on the second symmetry breaking scale F. Therefore, it is worthwhile to examine the dependence of a_τ on the scale F. Thus, in Fig. 5(a), we show the level of sensitivity exhibited by the τ AMDM when varying the F energy scale while keeping the f scale fixed, the fixed values assigned to the f scale are 1000, 2000 and 3000 GeV. For the three distinct energy scales, we find that the numerical predictions in the τ AMDM are $\mathrm{Re}[a_\tau] = [2.36 \times 10^{-9}, 6.54 \times 10^{-10}]$, $\mathrm{Re}[a_\tau] = [1.80 \times 10^{-9}, 5.89 \times 10^{-10}]$ and $\mathrm{Re}[a_\tau] = [1.30 \times 10^{-9}, 5.21 \times 10^{-10}]$, respectively. It is important to note that these contributions to a_τ acquire only real values and are all of the same order of magnitude, $10^{-9} - 10^{-10}$. These values decrease drastically as the F scale increases up to 6000 GeV. As we observed in the plot, the dominant contribution arises for small values of the f scale, particularly when $f = 1000$ GeV. Concerning, Fig. 5(b), we plot the curves of the contributions to a_τ in the analysis range of $f = [1000, 3000]$ GeV, now we fix the scale F and assign values such as 3000, 4000, 5000 and 6000 GeV. For these fixed values of F, we explore the sensitivity of $\mathrm{Re}(a_\tau)$ and find that the corresponding numerical estimates are $\mathrm{Re}[a_\tau] = [2.36, 1.30] \times 10^{-9}$, $\mathrm{Re}[a_\tau] = [1.40 \times 10^{-9}, 9.37 \times 10^{-10}]$, $\mathrm{Re}[a_\tau] = [9.21, 6.89] \times 10^{-10}$ and $\mathrm{Re}[a_\tau] = [6.54, 5.21] \times 10^{-10}$. Again, $\mathrm{Re}[a_\tau] \sim 10^{-9} - 10^{-10}$ and also acquires large values for small values of the F scale, this being $F = 3000$ GeV. By comparison, we find that $\mathrm{Re}[a_\tau]$ takes values of the same order of magnitude if F is varied while f is fixed or the opposite. Although specifically, $\mathrm{Re}[a_\tau]$ obtains larger values when $f = 1000$ GeV or $F = 3000$ GeV.

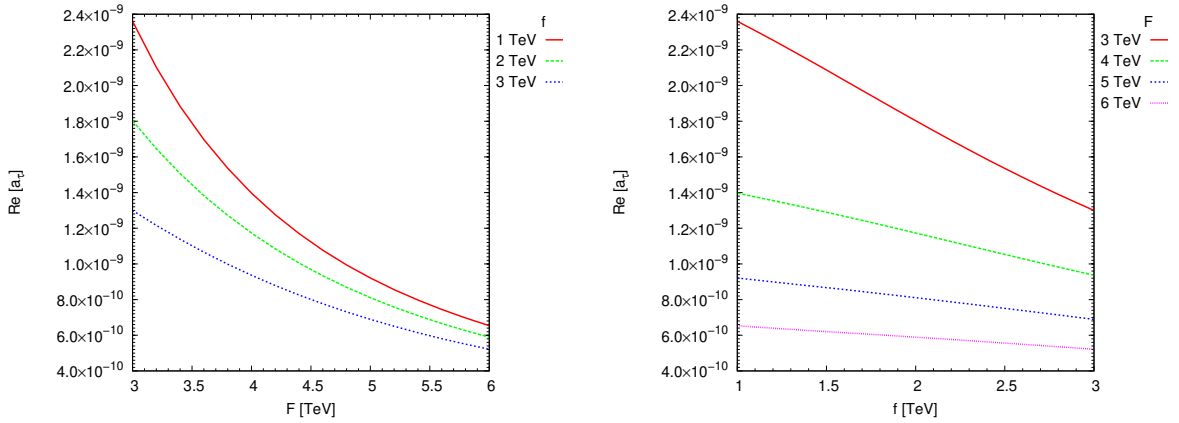

(a) (b)

FIG. 5: a) Total contribution to Re(a_τ) for different values of the energy scale f. b) Total contribution to Re(a_τ) for different values of the energy scale F. The plots are obtained for specific fixed values of the f or F scale. The values provided in Table III are used for the remaining parameters of the model.

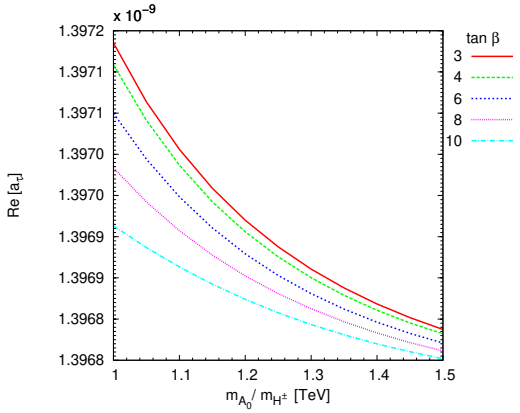

(a)

FIG. 6: Total contribution to Re(a_τ) for different values of tan β. The plot is obtained with fixed values of the $f = 1000$ GeV and $F = 4000$ GeV. The values provided in Table III are used for the remaining parameters of the model.

We now turn to examine the behavior of the real part of a_τ as a function of the mass of the pseudoscalar A_0 or the charged scalar $H^\pm$, which by the particular characteristics of the BLHM $m_{A_0} = m_{H^\pm}$. In this case, we are interested in investigating the phenomenological

details associated with the increase of m_{A_0} (or $m_{H^\pm}$) vs. Re$[a_\tau]$. According to Eq. (50), the parameter $\tan\beta$ is directly related to m_{A_0}, since the range of values that $\tan\beta$ could take is established precisely by the value assigned to m_{A_0}, i.e., for $m_{A_0} = 1000$ GeV and $m_{A_0} = 1500$ GeV the respective ranges of values for the parameter $\tan\beta$, $\tan\beta \in (1, 10.45)$ and $\tan\beta \in (1, 11.99)$ are generated. To evaluate the numerical contributions of Re$[a_\tau]$, we propose to vary the m_{A_0} parameter from 1000 GeV to 1500 GeV and also take certain values of $\tan\beta$ in the allowed value space, that is, $\tan\beta = 3, 4, 6, 8$ and 10. Fig. 6 shows the dependence of Re$[a_\tau]$ on m_{A_0}, we observe that the main signal is reached for $\tan\beta = 3$ while the lowest signal is obtained for $\tan\beta = 10$, Re$[a_\tau] = [1.3971, 1.3968] \times 10^{-9}$ and Re$[a_\tau] = [1.3969, 1.3967] \times 10^{-9}$, respectively. For the remaining curves, Re$[a_\tau] \sim 10^{-9}$. According to our predictions, Re$[a_\tau]$ shows a dependence on the m_{A_0} parameter. However, Re$[a_\tau]$ has a small sensitivity to changes in the parameter $\tan\beta$ since the numerical values obtained by Re$[a_\tau]$ are of the same order of magnitude for different choices in the values of $\tan\beta$.

TABLE IV: The magnitude of the partial contributions to a_τ of the BLHM. The data are obtained by fixing the f and F scales, $f = 1000$ GeV and $F = 4000$ GeV. The values provided in Table III are used for the rest of the model parameters. **abc** denotes the different particles running in the loop of the vertex $\gamma\tau^+\tau^-$.

$f = 1000$ GeV, $F = 4000$ GeV	
Couplings **abc**	$(a_\tau)^{\mathbf{abc}}$
$\sigma\tau\tau$	$-2.09 \times 10^{-14} + 0\,i$
$A_0\tau\tau$	$2.72 \times 10^{-12} + 0\,i$
$H_0\tau\tau$	$-2.24 \times 10^{-12} + 0\,i$
$\eta^0\tau\tau$	$2.22 \times 10^{-11} + 0\,i$
$\phi^0\tau\tau$	$1.07 \times 10^{-12} + 0\,i$
$Z'\tau\tau$	$3.92 \times 10^{-10} + 0\,i$
$W'^+W'^-\nu_\tau$	$9.81 \times 10^{-10} + 0\,i$

C. AWMDM of the tau-lepton at the BLHM

In this subsection, we perform the numerical estimation of the AWMDM a_τ^W ($a_\tau^W \equiv a_\tau^{W-BLHM}$) of the tau-lepton induced by a scalar, vector and scalar-vector bosons of the BLHM depicted in Figs. 2(a), 2(b)-2(c) and 2(d)-2(e), respectively. As in Subsection IV B, in the $\tan\theta_g = 1$ scenario implying that $\sin\theta_g = \cos\theta_g$ leads to the cancellation of some Feynman diagrams in Figs. 2(d)-2(e), this is because the Feynman rules for the involved vertices $ZW^+\phi^-$, $ZW^+\eta^-$ and $Z_\mu Z'_\nu H_i$ are made zero by the condition mentioned above (see Table X in Appendix A). The remaining Feynman diagrams provide non-zero contributions to a_τ^W.

In this sense, we start by showing in Fig. 7 the contributions of the different scalars to the τ AWMDM, here and in the subsequent cases a_τ^W acquire a real part and an imaginary part. We plot the behavior of a_τ^W as a function of the new physical scale f for the interval $f = [1000, 3000]$ GeV, while the other parameters assume fixed values. In the left plot of Fig. 7, it can see that the great majority of the scalars involved generate positive contributions to $\mathrm{Re}\,[a_\tau^W]$, and only the H_0 and σ scalars contribute negatively. Of all the scalars, the heaviest of them is σ and it contributes quite small values to $\mathrm{Re}\,[a_\tau^W]$, $|\mathrm{Re}\,[a_\tau^W(\sigma)]| = [5.16 \times 10^{-16}, 8.20 \times 10^{-18}]$. In contrast, the scalars $\eta^\pm$ and $H^\pm$ generate the main contributions to $\mathrm{Re}\,[a_\tau^W]$ in the range of analysis established for the f energy scale, i.e, $\mathrm{Re}\,[a_\tau^W(\eta^\pm)] = [1.38 \times 10^{-13}, 9.51 \times 10^{-14}]$ for the interval $f = [1000, 1100]$ GeV and $\mathrm{Re}\,[a_\tau^W(H^\pm)] = (9.51, 9.35] \times 10^{-14}$ for $f = (1100, 3000]$ GeV. Concerning the right plot of Fig. 7, it can observe that again the H_0 and σ scalars contribute negatively, in this case to $\mathrm{Im}\,(a_\tau^W)$, while the rest of the scalars contribute positively. The η^0 scalar provides the largest contributions to $\mathrm{Im}\,[a_\tau^W]$, while the smallest contribution is induced by σ: $\mathrm{Im}\,[a_\tau^W(\eta^0)] = [3.28 \times 10^{-13}, 3.58 \times 10^{-14}]$ and $|\mathrm{Im}\,[a_\tau^W(\sigma)]| = [1.14 \times 10^{-16}, 1.38 \times 10^{-18}]$.

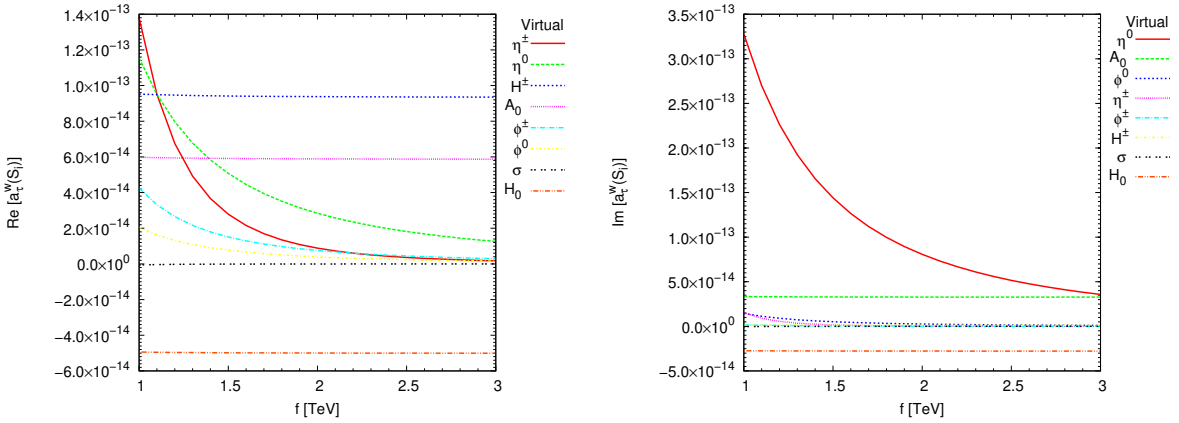

(a) (b)

FIG. 7: Individual scalar contributions to a_τ^W. a) Re(a_τ^W). b) Im(a_τ^W). The plots are obtained with the fixed value of $F = 4000$ GeV. The values provided in Table III are used for the remaining model parameters.

We discuss the contributions induced by the vector and scalar-vector bosons to the τ AWMDM. We begin by examining the real and imaginary parts of the BLHM partial contributions to a_τ^W. Thus, from Fig. 8, we can see that all the generated contributions are positive except the real part of the scalar-vector contribution, induced by Z and H_0. The dominant contributions for both the real and imaginary part of a_τ^W are achieved when the vector boson $W'^\pm$ circulates in the $Z\tau^+\tau^-$ vertex loop. In this case, the corresponding numerical contributions are $\text{Re}[a_\tau^W(W'^\pm)] = [2.72, 1.85] \times 10^{-9}$ and $\text{Im}[a_\tau^W(W'^\pm)] = [9.01, 4.16] \times 10^{-13}$. Other subdominant contributions appear when particles $W'^+\phi^-$, $\phi^+W'^-$ and Z' circulate in the above-mentioned vertex loop: $\text{Re}[a_\tau^W(W'^+\phi^-)] = \text{Re}[a_\tau^W(\phi^+W'^-)] = [4.67, 3.23] \times 10^{-10}$ and $\text{Im}[a_\tau^W(Z')] = [2.42, 1.12] \times 10^{-13}$. Complementarily, the minor contributions arise for the following cases: $|\text{Re}[a_\tau^W(ZH_0)]| = [5.69, 5.83] \times 10^{-12}$ and $\text{Im}[a_\tau^W(ZH_0)] = \text{Im}[a_\tau^W(W'^+\phi^-)] = \text{Im}[a_\tau^W(W'^+\eta^-)] = 0$. If we compare our numerical estimates, we find that the real parts of the partial contributions provide significant contributions to a_τ^W since they are at least one order of magnitude larger than the imaginary parts. In Table V, we show the magnitudes of all partial contributions to a_τ^W that correspond to the virtual particles circulating in the $Z\tau^+\tau^-$ vertex loop.

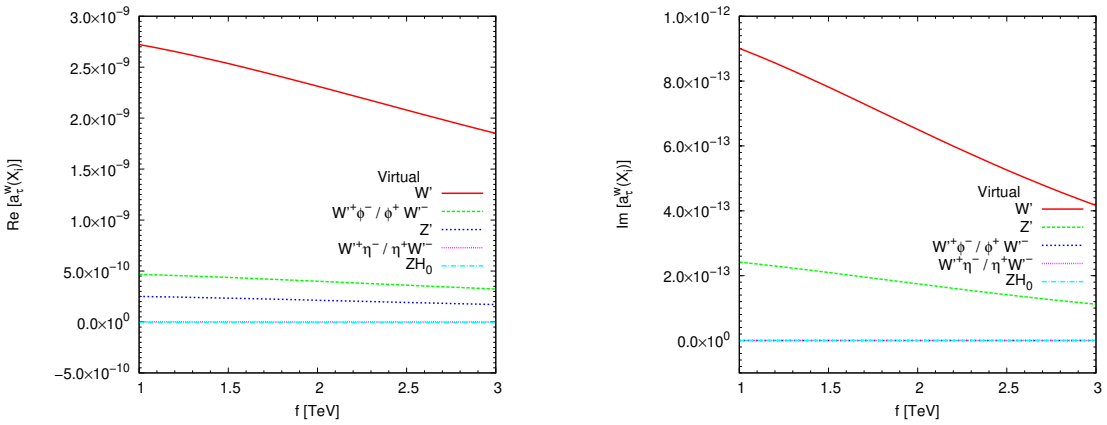

(a) (b)

FIG. 8: Individual vector and scalar-vector contributions to a_τ^W. a) Re(a_τ^W). b) Im(a_τ^W). The plots are obtained with the fixed value of $F = 4000$ GeV. The values provided in Table III are used for the remaining model parameters.

In the following, we show the curves that represent the sum of all individual contributions due to the scalar and vector bosons and the scalar-vector contributions. The magnitude of these contributions is shown in Fig. 9. Here, we observe that the total vector contribution dominates over the scalar and scalar-vector contributions since the latter are suppressed. With respect to the real part of a_τ^W depicted in Fig. 9(a), we can observe more closely that Re$[a_\tau^W(\text{total})]$ and Re$[a_\tau^W(\text{vector})]$ obtain values of the same order of magnitude, 10^{-9}, while Re$[a_\tau^W(\text{s-v})] \sim 10^{-10}$ and Re$[a_\tau^W(\text{scalar})] \sim 10^{-13}$. With the imaginary part of a_τ^W (see Fig. 9(b)) the same happens as the real part, in this case, Im$[a_\tau^W(\text{total})] \sim$ Im$[a_\tau^W(\text{vector})] \sim 10^{-12} - 10^{-13}$, Im$[a_\tau^W(\text{scalar})] \sim 10^{-13} - 10^{-14}$ and Im$[a_\tau^W(\text{s-v})] = 0$. It is worth mentioning that Figs. 9(a) and 9(b) were obtained for a fixed value of the other physical scale of the BLHM, $F = 4000$ GeV, which is also involved in our calculations. We later present the sensitivity of a_τ^W for other values of the F scale.

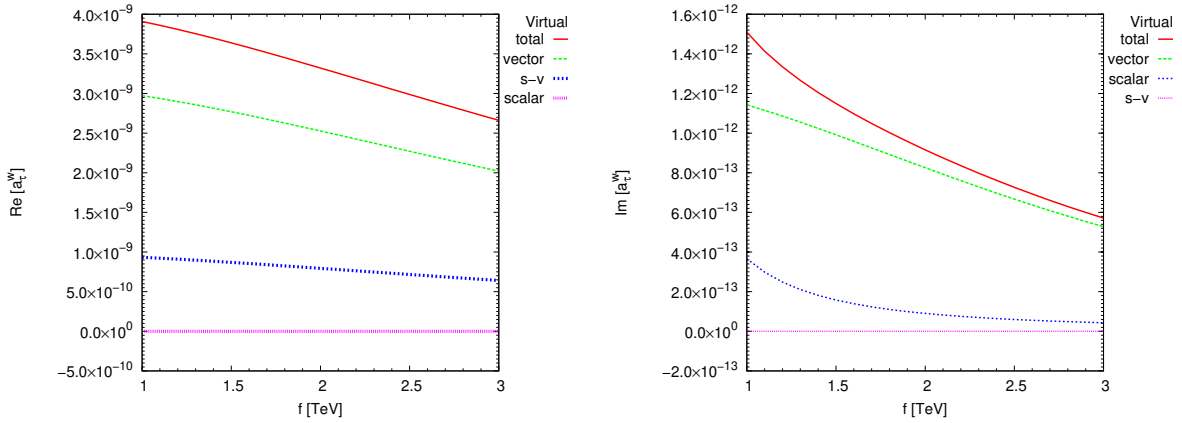

(a) (b)

FIG. 9: Scalar-vector (s-v), scalar, vector, and total contributions to a_τ^W. a) Re(a_τ^W). b) Im(a_τ^W). The plots are obtained with the fixed value of $F = 4000$ GeV. The values provided in Table III are used for the remaining model parameters.

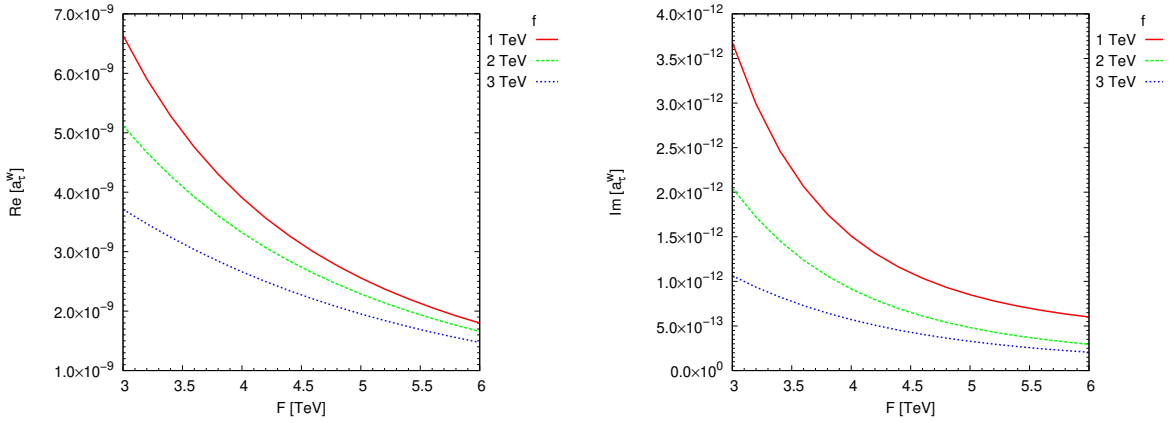

(a) (b)

FIG. 10: Total contribution to a_τ^W for different values of the energy scale f. a) Re(a_τ^W). b) Im(a_τ^W). The plots are obtained for specific fixed values of the f scale. The values provided in Table III are used for the remaining parameters of the model.

As already commented, the BLHM is based on two distinct global symmetries that break into diagonal subgroups at different scales, f and $F > f$. These scales represent the scales of the new physics. Therefore, it is very convenient to analyze the behavior of the τ AWMDM as a function of these energy scales since the masses of the new scalar and vector bosons strongly

depend on them. Thus, similar to what was performed in the previous subsection, we study the dependence of a_τ^W on F while maintaining fixed the f scale or the opposite. In Fig. 10, we begin by showing a variation of the scale F from 3000 GeV to 6000 GeV for three different f energy scales, i.e., $f = 1000$ GeV, 2000 GeV, 3000 GeV. In this plot, we appreciate that the main contributions to a_τ^W arise for $f = 1000$ GeV. This occurs for both the real and the imaginary part of a_τ^W: $\text{Re}[a_\tau^W] = [6.64, 1.80] \times 10^{-9}$ and $\text{Im}[a_\tau^W] = [3.68 \times 10^{-12}, 6.00 \times 10^{-13}]$, respectively. On the other hand, the weakest contributions appear when the scale f takes larger values, especially when $f = 3000$ GeV: $\text{Re}[a_\tau^W] = [3.71, 1.47] \times 10^{-9}$ and $\text{Im}[a_\tau^W] = [1.06 \times 10^{-12}, 2.05 \times 10^{-13}]$.

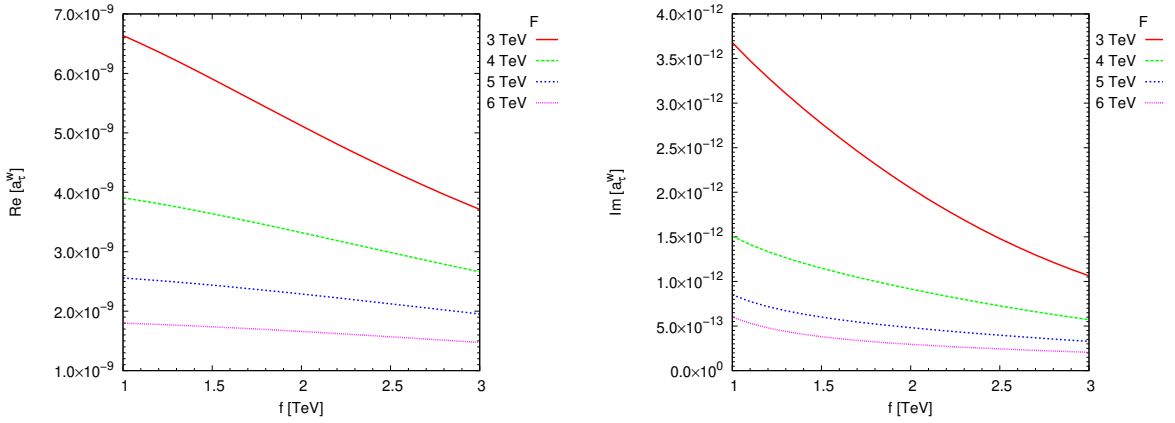

(a) (b)

FIG. 11: Total contribution to a_τ^W for different values of the energy scale F. a) $\text{Re}(a_\tau^W)$. b) $\text{Im}(a_\tau^W)$. The plots are obtained for certain fixed values of the F scale. The values provided in Table III are used for the remaining parameters of the model.

Now, we examine the dependence of a_τ^W on the f scale for certain fixed values of the F scale, i.e., $F = 3000$ GeV, 4000 GeV, 5000 GeV, 6000 GeV. With these values of F, we plot the curves shown in Fig. 11. In this case, the largest contributions to a_τ^W are reached for $F = 3000$ GeV, these contributions are $\text{Re}[a_\tau^W] = [6.64, 3.71] \times 10^{-9}$ and $\text{Im}[a_\tau^W] = [3.68, 1.06] \times 10^{-12}$. On the opposite side, the smallest contributions to a_τ^W are generated when $F = 6000$ GeV: $\text{Re}[a_\tau^W] = [1.80, 1.47] \times 10^{-9}$ and $\text{Im}[a_\tau^W] = [6.00, 2.05] \times 10^{-13}$.

According to the numerical results, it is found that a_τ^W is sensitive to a slight change in the values of the f and F scales, this occurs as long as these parameters are in the established intervals. When a_τ^W depends on F, we observe that a_τ^W has a decrease of about one order

of magnitude as F increases up to 6000 GeV. For the following case, when a_τ^W depends on f, we also have a decrease of at most one order of magnitude as f reaches 3000 GeV. In summary, we can affirm that a_τ^W gets large values when $f = 1000$ GeV or $F = 3000$ GeV, while smaller values are obtained for a_τ^W when the scales tend to take values close to their established upper limits. In short, $a_\tau^W = 6.64 \times 10^{-9} + 3.68 \times 10^{-12}\, i$ is the largest value found when $f = 1000$ GeV and $F = 3000$ GeV.

Finally, Fig. 12 show the a_τ^W behavior as a function of m_{A_0} or $m_{H^\pm}$, for $\tan\beta = 3$, 4, 6, 8 and 10. From this figure, we can observe that the largest contributions to the τ AWMDM arise when $\tan\beta = 3$. This happens for the real and imaginary part of a_τ^W: $\mathrm{Re}[a_\tau^W] = [3.91307, 3.91301] \times 10^{-9}$ and $\mathrm{Im}[a_\tau^W] = [1.50892, 1.50353] \times 10^{-12}$. As the parameter, $\tan\beta$, increases more suppressed curves are generated. This occurs in the case of $\tan\beta = 10$ which gives the following values corresponding to a_τ^W, $\mathrm{Re}[a_\tau^W] = [3.91298, 3.91297] \times 10^{-9}$ and $\mathrm{Im}[a_\tau^W] = [1.50500, 1.50288] \times 10^{-12}$. Furthermore, a_τ^W acquires smaller values as the mass of the pseudoscalar A_0 increases up to 1500 GeV. However, we can say that the changes or effects on a_τ^W are not so great since the numerical values they acquire remain of the same order of magnitude.

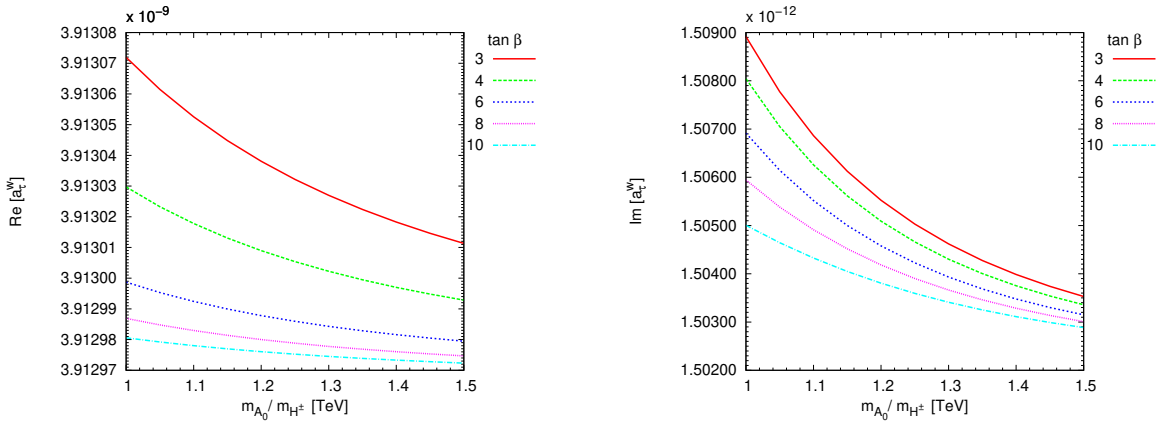

(a) (b)

FIG. 12: Total contribution to a_τ^W for different values of $\tan\beta$. a) $\mathrm{Re}(a_\tau^W)$. b) $\mathrm{Im}(a_\tau^W)$. The plots are obtained for fixed values of the $f = 1000$ GeV and $F = 4000$ GeV. The values provided in Table III are used for the remaining parameters of the model.

TABLE V: The magnitude of the partial contributions to a_τ^W of the BLHM. The data are obtained by fixing the f and F scales, $f = 1000$ GeV and $F = 4000$ GeV. The values provided in Table III are used for the rest of the model parameters. **abc** denotes the different particles running in the loop of the vertex $Z\tau^+\tau^-$.

$f = 1000$ GeV, $F = 4000$ GeV	
Couplings **abc**	$\left(a_\tau^W\right)^{\mathbf{abc}}$
$\sigma\tau\tau$	$-2.83 \times 10^{-16} - 1.14 \times 10^{-16}\ i$
$A_0\tau\tau$	$5.98 \times 10^{-14} + 3.33 \times 10^{-14}\ i$
$H_0\tau\tau$	$-4.94 \times 10^{-14} - 2.74 \times 10^{-14}\ i$
$\eta^0\tau\tau$	$1.15 \times 10^{-13} + 3.28 \times 10^{-13}\ i$
$\phi^0\tau\tau$	$2.05 \times 10^{-14} + 1.44 \times 10^{-14}\ i$
$H^\pm\nu_\tau\nu_\tau$	$9.52 \times 10^{-14} + 1.21 \times 10^{-15}\ i$
$\eta^\pm\nu_\tau\nu_\tau$	$1.38 \times 10^{-13} + 1.53 \times 10^{-14}\ i$
$\phi^\pm\nu_\tau\nu_\tau$	$4.25 \times 10^{-14} + 1.65 \times 10^{-15}\ i$
$Z'\tau\tau$	$2.51 \times 10^{-10} + 2.42 \times 10^{-13}\ i$
$W'^\pm\nu_\tau\nu_\tau$	$9.33 \times 10^{-10} + 9.01 \times 10^{-13}\ i$
$W'^+W'^-\nu_\tau$	$1.79 \times 10^{-9} + 0\ i$
$W'^+\phi^-\nu_\tau$	$4.67 \times 10^{-10} + 0\ i$
$\phi^+W'^-\nu_\tau$	$4.67 \times 10^{-10} + 0\ i$
$W'^+\eta^-\nu_\tau$	$2.34 \times 10^{-12} + 0\ i$
$\eta^+W'^-\nu_\tau$	$2.34 \times 10^{-12} + 0\ i$
$ZH_0\tau$	$-5.69 \times 10^{-12} + 0\ i$

D. Contributions of the SM and BLHM to the AMDM and AWMDM of the tau-lepton

As previously defined (Eqs. (48) and (49)), the contribution of the SM and BLHM particles to the AMDM and AWMDM of the tau-lepton will be represented by α_τ and α_τ^W, respectively. In this way, in Tables VI and VII we provide the partial and total numerical values for α_τ and α_τ^W. In these tables, we find that all new diagrams arising in the BLHM

have a small numerical impact on the AMDM and AWMDM of the τ-lepton. This is partly because both a_τ and a_τ^W acquire values inversely proportional to the energy scales f and F. Only some partial contributions are comparable to the SM partial contributions (see Appendix B) but not larger than them. The SM particles provide the largest contributions to α_τ and α_τ^W. According to the numerical data, we find that $\alpha_\tau = 116090.46 \times 10^{-8}$ and $\alpha_\tau^W = -1.92 \times 10^{-6} - 0.57 \times 10^{-6}\, i$.

TABLE VI: Partial contributions to α_τ. **abc** denotes the different particles running in the loop of the vertex $\gamma\tau^+\tau^-$.

$f = 1000$ GeV, $F = 4000$ GeV	
Couplings **abc**	$(\alpha_\tau)^{\mathbf{abc}}$
$\gamma\tau\tau$	$116140.97 \times 10^{-8} + 0\, i$
$Z\tau\tau + Z'\tau\tau$	$51.59 \times 10^{-8} + 0\ i$
$h_0\tau\tau + A_0\tau\tau + H_0\tau\tau + \phi^0\tau\tau + \eta^0\tau\tau + \sigma\tau\tau$	$0.09 \times 10^{-8} + 0\ i$
$\nu_\tau W^+W^- + \nu_\tau W'^+W'^-$	$-102.19 \times 10^{-8} + 0\ i$
Total	$\alpha_\tau = 116090.46 \times 10^{-8} + 0\ i$

TABLE VII: Partial contributions to α_τ^W. **abc** denotes the different particles running in the loop of the vertex $Z\tau^+\tau^-$.

$f = 1000$ GeV, $F = 4000$ GeV	
Couplings **abc**	$\left(\alpha_\tau^W\right)^{\mathbf{abc}}$
$\gamma\tau\tau$	$3.09 \times 10^{-7} - 1.24 \times 10^{-7}\, i$
$Z\tau\tau + Z'\tau\tau$	$4.05 \times 10^{-8} + 1.86 \times 10^{-8}\ i$
$h_0\tau\tau + A_0\tau\tau + H_0\tau\tau + \phi^0\tau\tau + \eta^0\tau\tau + \sigma\tau\tau$	$-6.58 \times 10^{-12} - 1.34 \times 10^{-11}\ i$
$W^\pm\nu_\tau\nu_\tau + W'^\pm\nu_\tau\nu_\tau + H^\pm\nu_\tau\nu_\tau + \phi^\pm\nu_\tau\nu_\tau + \eta^\pm\nu_\tau\nu_\tau$	$-9.13 \times 10^{-7} - 4.66 \times 10^{-7}\ i$
$\nu_\tau W^+W^- + \nu_\tau W'^+W'^-$	$-1.37 \times 10^{-6} + 0\ i$
$\tau h_0 Z + \tau H_0 Z$	$1.35 \times 10^{-8} + 0\ i$
$W'^+\phi^-\nu_\tau + \phi^+W'^-\nu_\tau + W'^+\eta^-\nu_\tau + \eta^+W'^-\nu_\tau$	$9.39 \times 10^{-10} + 0\ i$
Total	$\alpha_\tau^{\mathbf{W}} = -1.92 \times 10^{-6} - 0.57 \times 10^{-6}\ i$

V. CONCLUSIONS

We have calculated the contributions generated by the SM (see Appendix B) and BLHM particles to the AMDM and AWMDM of the tau-lepton at the one-loop level. Within the SM, we find that our predictions for a_τ^{SM} and a_τ^{W-SM} are in agreement with the results reported in the literature. Concerning the new physics, this arises in the BLHM scenario and is induced by the new scalar and vector bosons. The new contributions that these generate to a_τ and a_τ^W are emphasized.

The BLHM has two global symmetries that break at different energy scales, so f and F represent the scales of the new physics, and at this level, the new scalar and vector bosons acquire their respective masses. Therefore, we have analyzed the dependence of a_τ and a_τ^W on the physical scales f and F, and we find that both a_τ and a_τ^W are sensitive to changes in f and F. Large values of these energy scales, as long as they are in the allowed intervals, suppress the contributions to a_τ and a_τ^W. However, when these scales acquire the respective minimum values, $f = 1000$ GeV and $F = 3000$ GeV, large values are reached for the τ AMDM and AWMDM: $a_\tau = 2.36 \times 10^{-9} + 0\,i$ and $a_\tau^W = 6.64 \times 10^{-9} + 3.68 \times 10^{-12}\,i$, respectively. In this work, we also examine the dependence of a_τ and a_τ^W on the m_{A_0} parameter. Our results indicate that both show a small sensitivity to changes in the m_{A_0} parameter since the contributions they acquire remain of the same order of magnitude, $a_\tau \sim 10^{-9}$ and $a_\tau^W \sim 10^{-9}$.

It is interesting to study the contributions of the new physics as they could significantly improve the AMDM and AWMDM of the tau-lepton. This is because, for now, the sensitivity reached by the colliders is beyond the level of precision required to test the SM predictions on a_τ^{SM} and a_τ^{SM-W}. Therefore, it is worth studying the effects of new particles not described by the SM as they could generate potentially significant contributions and be within reach of future experimental measurements. In the BLHM scenario, we found that the contributions generated by the new scalar and vector bosons to the τ AMDM and AWMDM are $a_\tau \sim 10^{-9}$ and $a_\tau^W \sim 10^{-9}$. These numerical values are smaller than the SM contributions. However, they are similar in size and even more significant than those arising in some SM extensions, such as the Simplest Little Higgs model, $a_\tau \sim 10^{-9}$ and $a_\tau^W \sim 10^{-9}$ [52]; the Two-Higgs Doublet models (type-I and type-II), $a_\tau^W \sim 10^{-9} - 10^{-10}$ [53, 54]; the Two-Higgs Doublet models type-III with textures, $a_\tau \sim 10^{-7} - 10^{-8}$ and $a_\tau^W \sim 10^{-7} - 10^{-10}$ [55];

Scalar Leptoquark models, $a_\tau \sim 10^{-9}$ and $a_\tau^W \sim 10^{-9}$ [56]; the Minimal Supersymmetric Standard Model with a mirror fourth generation, $a_\tau \sim 10^{-6} - 10^{-10}$ [57]; unparticle physics (for $\bigwedge_U = 10$ TeV), $a_\tau \sim 10^{-9} - 10^{-10}$ and $a_\tau^W \sim 10^{-9} - 10^{-10}$ [58]; the type-I and type-III seesaw models, $|a_\tau^I| < 1.87 \times 10^{-8}$ and $|a_\tau^{III}| < 7.55 \times 10^{-9}$ [59]; and finally, in the framework of the effective lagrangian approach and the Fritzsch-Xing lepton mass matrix, $a_\tau \sim 10^{-11}$ [60].

Currently, the experimental limits in the τ AMDM and AWMDM are well above theoretical predictions. Our results are also outside the detection range of future experiments, so there is insufficient sensitivity to be tested and cross-checked with experimental values. The results presented here complement other studies performed on models with an extended scalar sector and may be helpful to the scientific community.

Acknowledgements

E. C. A. appreciates the post-doctoral stay. A. G. R. thank SNI and PROFEXCE (México).

Appendix A: The Feynman rules for the BLHM

In this appendix, we present the Feynman rules for the BLHM involved in our calculation for the AMDM and AWMDM of the tau-lepton. It is convenient to define the following useful notation:

$$c_\beta = \cos\beta, \tag{A1}$$

$$s_\beta = \sin\beta, \tag{A2}$$

$$s_\alpha = \sin\alpha, \tag{A3}$$

$$c_\alpha = \cos\alpha, \tag{A4}$$

$$c_g = \cos\theta_g, \tag{A5}$$

$$s_g = \sin\theta_g, \tag{A6}$$

$$x_s = \frac{1}{2\cos\theta_W}\sin\theta_g\cos\theta_g(\sin^2\theta_g - \cos^2\theta_g), \tag{A7}$$

$$y_\tau = \frac{m_\tau}{v\sin\beta}\left(1 - \frac{v^2}{3f^2}\right)^{-1/2}. \tag{A8}$$

TABLE VIII: Feynman rules for the BLHM involving the escalars σ, h_0, H_0, ϕ^0, η^0, $H^\pm$, $\phi^\pm$, $\eta^\pm$, the pseudoscalar A_0 and the vector bosons Z' and $W'^\pm$.

Vertex	**Couplings**
$\sigma\bar{\tau}\tau$	$\frac{c_\beta v y_\tau}{\sqrt{2}f}$
$h_0\bar{\tau}\tau$	$c_\alpha y_\tau - \frac{\left(16c_\beta s_\alpha s_\beta v^2 + c_\alpha\left(8c_\beta^2 v^2 + 24 s_\beta^2 v^2\right)\right)y_\tau}{24f^2}$
$H_0\bar{\tau}\tau$	$-s_\alpha y_\tau + \frac{\left(s_\alpha c_\beta^2 - 2c_\alpha s_\beta c_\beta + 3 s_\alpha s_\beta^2\right)v^2 y_\tau}{3f^2}$
$A_0\bar{\tau}\tau$	$-ic_\beta y_\tau$
$\eta^0\bar{\tau}\tau$	$-\frac{is_\beta v y_\tau}{2f}$
$\phi^0\bar{\tau}\tau$	$\frac{is_\beta v y_\tau}{2f}$
$H^+\bar{\nu}_\tau\tau$	$\sqrt{2}c_\beta y_\tau P_R$
$\eta^+\bar{\nu}_\tau\tau$	$\frac{is_\beta v y_\tau}{\sqrt{2}f}P_R$
$\phi^+\bar{\nu}_\tau\tau$	$-\frac{is_\beta v y_\tau}{\sqrt{2}f}P_R$
$Z'\bar{\tau}\tau$	$\frac{1}{2}ig\gamma^\mu P_L$
$W'^+\bar{\nu}_\tau\tau$	$-\frac{ig}{\sqrt{2}}\gamma^\mu P_L$

TABLE IX: Self-couplings of gauge bosons in the BLHM.

Vertex	**Couplings**
$Z_\mu(q)W'^-_\alpha(k)W'^+_\beta(p)$	$ig\,c_W\left[\delta_{\beta\mu}\left(p_\alpha-q_\alpha\right)+\delta_{\alpha\mu}\left(q_\beta-k_\beta\right)+\delta_{\alpha\beta}\left(k_\mu-p_\mu\right)\right]$ $-\frac{g\,v^2x_s(2\,c_g^2-2\,s_g^2-c_gs_gc_W(2c_W+1))}{2c_gs_g(f^2+F^2)}[\delta_{\beta\mu}\left(p_\alpha-q_\alpha\right)+\delta_{\alpha\mu}\left(q_\beta-k_\beta\right)$ $+\delta_{\alpha\beta}\left(k_\mu-p_\mu\right)]$
$A_\mu(q)W'^-_\alpha(k)W'^+_\beta(p)$	$ig\,s_W\left[\delta_{\alpha\beta}\left(k_\mu-p_\mu\right)+\delta_{\beta\mu}\left(p_\alpha-q_\alpha\right)+\delta_{\alpha\mu}\left(q_\beta-k_\beta\right)\right]$ $-\frac{g\,v^2c_Ws_Wx_s}{(f^2+F^2)}\left[\delta_{\alpha\beta}\left(k_\mu-p_\mu\right)+\delta_{\beta\mu}\left(p_\alpha-q_\alpha\right)+\delta_{\alpha\mu}\left(q_\beta-k_\beta\right)\right]$

TABLE X: Three-point couplings of two gauge bosons to a scalar in the BLHM.

Vertex	**Couplings**
$ZZ'h_0$	$-\frac{gs_Wv\left(c_g^2-s_g^2\right)\left(g^2+g'^2\right)\sin(\alpha+\beta)}{2c_gs_gg'}+\frac{gs_Wv^3\left(c_g^2-s_g^2\right)\left(g^2+g'^2\right)\sin(\alpha+\beta)}{6c_gs_gg'f^2}$ $+\frac{v^3x_s\sin(\alpha+\beta)\left(c_g^2gg's_W\left(g^2+g'^2\right)+2c_gs_g\left(g^4s_W^2+g^2g'^2\left(2s_W^2+1\right)+g'^4s_W^2\right)-gg's_g^2s_W\left(g^2+g'^2\right)\right)}{2c_gs_gg'^2(f^2+F^2)}$
ZZH_0	$\frac{s_W^2v\left(g^2+g'^2\right)^2\cos(\alpha+\beta)}{2g'^2}-\frac{s_W^2v^3\left(g^2+g'^2\right)^2\cos(\alpha+\beta)}{6g'^2f^2}$ $-\frac{s_Wv^3x_s\left(g^2+g'^2\right)\cos(\alpha+\beta)\left(c_g^2(-g)g'+c_gs_gs_W\left(g^2+g'^2\right)+gg's_g^2\right)}{2c_gs_gg'^2(f^2+F^2)}$
$ZZ'H_0$	$-\frac{gs_Wv\left(c_g^2-s_g^2\right)\left(g^2+g'^2\right)\cos(\alpha+\beta)}{2c_gs_gg'}+\frac{gs_Wv^3\left(c_g^2-s_g^2\right)\left(g^2+g'^2\right)\cos(\alpha+\beta)}{6c_gs_gg'f^2}$ $+\frac{v^3x_s\cos(\alpha+\beta)\left(c_g^2gg's_W\left(g^2+g'^2\right)+2c_gs_g\left(g^4s_W^2+g^2g'^2\left(2s_W^2+1\right)+g'^4s_W^2\right)-gg's_g^2s_W\left(g^2+g'^2\right)\right)}{2c_gs_gg'^2(f^2+F^2)}$
$A_\gamma W^+\eta^-$	$\frac{g^3s_W^2v^4x_s\left(c_g^2+s_g^2\right)}{8c_gs_gg'f(f^2+F^2)}$
$A_\gamma W'^+\eta^-$	$-\frac{g^2s_Wv^2\left(c_g^2+s_g^2\right)}{8c_gs_gf}+\frac{g^3s_W^2v^4x_s\left(c_g^2+s_g^2\right)}{16c_gs_gg'f(f^2+F^2)}$
$A_\gamma W^+\phi^-$	$\frac{fg^3s_W^2v^2x_s\left(c_g^2+s_g^2\right)}{2c_gs_gg'(f^2+F^2)}-\frac{g^3s_W^2v^4x_s\left(c_g^2+s_g^2\right)}{8c_gs_gg'f(f^2+F^2)}$
$A_\gamma W'^+\phi^-$	$-\frac{fg^2s_W\left(c_g^2+s_g^2\right)}{2c_gs_g}+\frac{g^2s_Wv^2\left(c_g^2+s_g^2\right)}{8c_gs_gf}+\frac{fg^3s_W^2v^2x_s\left(c_g^2+s_g^2\right)}{4c_gs_gg'(f^2+F^2)}-\frac{g^3s_W^2v^4x_s\left(c_g^2+s_g^2\right)}{16c_gs_gg'f(f^2+F^2)}$
$ZW^+\eta^-$	$-\frac{g^2s_W^2v^4x_s\left(c_g^2+s_g^2\right)}{8c_gs_gf(f^2+F^2)}$
$ZW'^+\eta^-$	$\frac{gg's_Wv^2\left(c_g^2+s_g^2\right)}{8c_gs_gf}-\frac{gs_Wv^4x_s\left(c_g^2+s_g^2\right)(gs_W+g')}{16c_gs_gf(f^2+F^2)}$
$ZW^+\phi^-$	$\frac{fg^2v^2x_s\left(c_g^2+s_g^2\right)\left(g^2s_W^2-g'^2\right)}{2c_gg'^2s_g(f^2+F^2)}-\frac{g^2v^4x_s\left(c_g^2+s_g^2\right)\left(2g^2s_W^2+g'^2\left(s_W^2-2\right)\right)}{8c_gs_gg'^2f(f^2+F^2)}$
$ZW'^+\phi^-$	$-\frac{fg^3s_W\left(c_g^2+s_g^2\right)}{2c_gs_gg'}+\frac{gs_Wv^2\left(c_g^2+s_g^2\right)\left(2g^2+g'^2\right)}{8c_gs_gg'f}+\frac{fg^3s_Wv^2x_s\left(c_g^2+s_g^2\right)(gs_W+g')}{4c_gs_gg'^2(f^2+F^2)}$ $-\frac{gs_Wv^4x_s\left(c_g^2+s_g^2\right)\left(2g^2+g'^2\right)(gs_W+g')}{16c_gs_gg'^2f(f^2+F^2)}$

Appendix B: The AMDM and AWMDM of the tau-lepton at the SM

In the SM, we estimate the contributions to the AMDM and AWMDM of the tau-lepton at the one-loop level. These contributions are calculated in the unitarity gauge so that the only Feynman diagrams that arise are those shown in Figs. 13 and 14. The first-order contributions for a_τ^{SM} and a_τ^{W-SM} are obtained from these figures.

The prediction of the AMDM of the τ-lepton in SM is calculated by considering only one-loop level contributions. In the literature, these contributions found are usually cataloged as the quantum electrodynamics (QED) contribution without hadrons and the electroweak contribution. In Table XI, we provide the numerical values of the QED contribution and the partial electroweak contributions. In this table, we can appreciate that indeed the QED contribution is the most important, followed by the electroweak contribution. Our result obtained on $a_\tau^{SM} = 116090.33 \times 10^{-8}$, is comparable to that of Ref. [26]. Regarding the EDM of the tau-lepton, it is absent at this level.

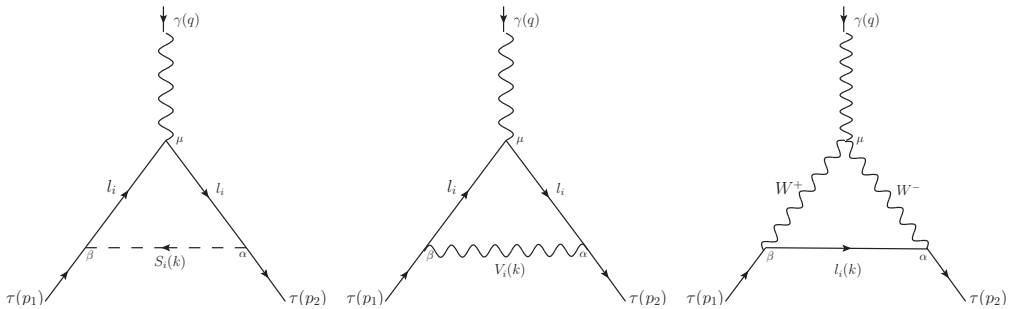

(a) (b) (c)

FIG. 13: Generic Feynman diagrams that contributes to the AMDM of the tau-lepton, $l_i \equiv \tau, \nu_\tau$. a) Scalar contribution, $S_i \equiv h_0$. b) and c) Vector contributions, $V_i \equiv \gamma, Z$.

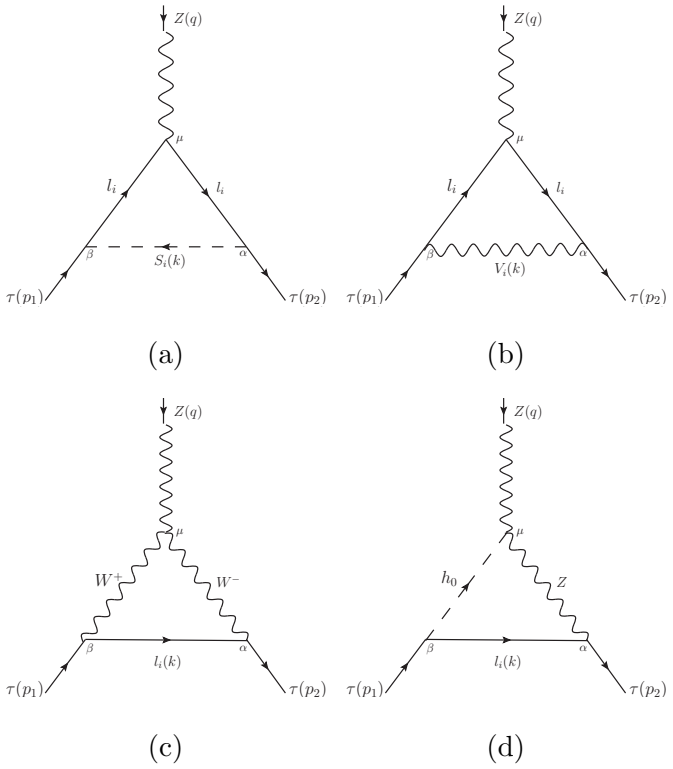

FIG. 14: Generic Feynman diagrams that contributes to the AWMDM of the tau-lepton, $l_i \equiv \tau, \nu_\tau$. a) Scalar contribution, $S_i \equiv h_0$. b) and c) Vector contributions, $V_i \equiv \gamma, Z$. d) Scalar-vector contribution.

TABLE XI: Partial contributions to a_τ^{SM}. **abc** denotes the different particles running in the loop of the vertex $\gamma\tau^+\tau^-$.

Couplings **abc**	$\left(a_\tau^{SM}\right)^{\mathbf{abc}}$
$\gamma\tau\tau$	$116140.97 \times 10^{-8} + 0\,i$
$Z\tau\tau$	$51.55 \times 10^{-8} + 0\ i$
$h_0\tau\tau$	$0.09 \times 10^{-8} + 0\ i$
$\nu_\tau W^+W^-$	$-102.29 \times 10^{-8} + 0\ i$
Total	$\mathbf{a_\tau^{SM}} = 116090.33 \times 10^{-8} + 0\ i$

We also estimate the AWMDM of the tau-lepton with the initial and final particles in the on-shell. The relevant diagrams in the unitary gauge are those shown in Fig. 14, and their numerical contributions are given in Table XII. In this table, we can appreciate that

the largest partial contribution to a_τ^{W-SM}, in absolute value, arises when W^+, W^- and ν_τ particles circulate in the loop. The total contribution to a_τ^{W-SM} is $-1.9193\times10^{-6}-0.5713\times 10^{-6}\ i$. Our result is comparable to that reported in Ref. [33], although a slight difference prevails. This is due to the fact that we used current values for the input parameters m_Z, m_W, m_τ, $\sin\theta_W$, and α (fine-structure constant).

TABLE XII: Partial contributions to a_τ^{W-SM}. **abc** denotes the different particles running in the loop of the vertex $Z\tau^+\tau^-$.

Couplings **abc**	$\left(a_\tau^{W-SM}\right)^{\mathbf{abc}}$
$\gamma\tau\tau$	$3.09\times10^{-7}-1.24\times10^{-7}\,i$
$Z\tau\tau$	$4.03\times10^{-8}+1.86\times10^{-8}\ i$
$h_0\tau\tau$	$-6.72\times10^{-12}-1.38\times10^{-11}\ i$
$W^\pm\nu_\tau\nu_\tau$	$-9.14\times10^{-7}-4.66\times10^{-7}\ i$
$\nu_\tau W^+W^-$	$-1.37\times10^{-6}+0\ i$
$\tau h_0 Z$	$1.35\times10^{-8}+0\ i$
Total	$\mathbf{a_\tau^{W-SM}}=-1.92\times10^{-6}-0.57\times10^{-6}\ i$

[1] I. Neutelings (ATLAS and CMS Collaboration), PoS **LHCP2020**, 045 (2021).

[2] ATLAS Collaboration, *Measurement of the tau lepton reconstruction and identification performance in the ATLAS experiment using pp collisions at* $\sqrt{s} = 13\ TeV$, ATLAS-CONF-2017-029.

[3] CMS Collaboration, *Performance of reconstruction and identification of tau leptons in their decays to hadrons and tau neutrino in LHC Run-2*, CMS-PAS-TAU-16-002.

[4] ATLAS Collaboration, *Reconstruction, Energy Calibration, and Identification of Hadronically Decaying Tau Leptons in the ATLAS Experiment for Run-2 of the LHC*, ATL-PHYS-PUB-2015-045.

[5] G. Aad, *et al.* (ATLAS Collaboration), *Eur. Phys. J.* C **75**, 303 (2015).

[6] A. Gutiérrez-Rodríguez, M. Köksal, A. A. Billur and M. A. Hernández-Ruíz, *Int. J. Theor. Phys.* **61**, 161 (2022).

[7] A. Gutiérrez-Rodríguez, C. Pérez-Mayorga and A. González-Sánchez, *Int. J. Theor. Phys.* **61**, 132 (2022).

[8] M. Dyndal, M. Klusek-Gawenda, M. Schott and A. Szczurek, *Phys. Lett.* B **809**, 135682 (2020).

[9] M. Köksal, A. A. Billur, A. Gutiérrez-Rodríguez and M. A. Hernández-Ruíz, *Int. J. Mod. Phys.* A **34**, 1950076 (2019).

[10] M. Köksal, A. A. Billur, A. Gutiérrez-Rodríguez and M. A. Hernández-Ruíz, *Phys. Rev.* D **98**, 015017 (2018).

[11] S. Eidelman, D. Epifanov, M. Fael, L. Mercolli and M. Passera, *JHEP* **03**, 140 (2016).

[12] S. Atağ and E. Gürkanlı, *JHEP* **06**, 118 (2016).

[13] A. Hayreter and G. Valencia, *Phys. Rev.* D **88**, 013015 (2013); Erratum: *Phys. Rev.* D **91**, 099902 (2015).

[14] A. Gutierrez-Rodriguez, M. A. Hernandez-Ruiz and C. P. Castaneda-Almanza, *J. Phys.* G **40**, 035001 (2013).

[15] A. Gutierrez-Rodriguez, *Mod. Phys. Lett.* A **25**, 703-713 (2010).

[16] M. Passera, *Nucl. Phys. B Proc. Suppl.* **169**, 213-225 (2007).

[17] A. Gutierrez-Rodriguez, M. A. Hernandez-Ruiz and M. A. Perez, *Int. J. Mod. Phys.* A **22**,

3493-3508 (2007).

[18] A. Gutierrez-Rodriguez, M. A. Hernandez-Ruiz and L. N. Luis-Noriega, *Mod. Phys. Lett.* A **19**, 2227 (2004).

[19] A. Pich, *Prog. Part. Nucl. Phys.* **75**, 41-85 (2014).

[20] G. Aad, *et al.* (ATLAS Collaboration), *Eur. Phys. J.* C **73**, 2328 (2013).

[21] P. A. Zyla, *et al.* (Particle Data Group), *Prog. Theor. Exp. Phys.* **2020**, 083C01 (2020).

[22] J. Abdallah, *et al.* (DELPHI Collaboration), *Eur. Phys. J.* C **35**, 159-170 (2004).

[23] K. Inami, *et al.* (Belle Collaboration), *Phys. Lett.* B **551**, 16-26 (2003).

[24] M. A. Samuel, G. w. Li and R. Mendel, *Phys. Rev. Lett.* **67**, 668-670 (1991); Erratum: *Phys. Rev. Lett.* **69**, 995 (1992).

[25] F. Hamzeh and N. F. Nasrallah, *Phys. Lett.* B **373**, 211-214 (1996).

[26] S. Eidelman and M. Passera, *Mod. Phys. Lett.* A **22**, 159-179 (2007).

[27] F. Hoogeveen, *Nucl. Phys.* B **341**, 322-340 (1990).

[28] M. E. Pospelov and I. B. Khriplovich, *Sov. J. Nucl. Phys.* **53**, 638-640 (1991).

[29] S. M. Barr and W. Marciano, in *CP violation*, edited by C. Jarlskog (World Scientific Singapore, 1990).

[30] A. Heister, *et al.* (ALEPH Collaboration), *Eur. Phys. J.* C **30**, 291-304 (2003).

[31] M. Acciarri, *et al.* (L3 Collaboration), *Phys. Lett.* B **426**, 207-216 (1998).

[32] K. Ackerstaff, *et al.* (OPAL Collaboration), *Z. Phys.* C **74**, 403-412 (1997).

[33] J. Bernabeu, G. A. Gonzalez-Sprinberg, M. Tung and J. Vidal, *Nucl. Phys.* B **436**, 474-486 (1995).

[34] W. Bernreuther, U. Low, J. P. Ma and O. Nachtmann, *Z. Phys.* C **43**, 117 (1989).

[35] N. Arkani-Hamed, A. G. Cohen and H. Georgi, *Phys. Lett.* **B513**, 232 (2001).

[36] N. Arkani-Hamed, A. G. Cohen, E. Katz, A. E. Nelson, T. Gregoire and J. G. Wacker, *JHEP* **08**, 021 (2002).

[37] N. Arkani-Hamed, A. G. Cohen, E. Katz and A. E. Nelson, *JHEP* **07**, 034 (2002).

[38] C. Csaki, J. Hubisz, G. D. Kribs, P. Meade and J. Terning, *Phys. Rev.* **D67**, 115002 (2003).

[39] C. Csaki, J. Hubisz, G. D. Kribs, P. Meade and J. Terning, *Phys. Rev.* **D68**, 035009 (2003).

[40] J. A. Casas, J. R. Espinosa and I. Hidalgo, *JHEP* **03**, 038 (2005).

[41] M. Schmaltz, D. Stolarski and J. Thaler, *JHEP* **09**, 018 (2010).

[42] P. Kalyniak, T. Martin and K. Moats, *Phys. Rev.* **D91**, 013010 (2015).

[43] D. Eriksson, J. Rathsman and O. Stal, *Comput. Phys. Commun.* **181**, 189 (2010).

[44] K. P. Moats, *Phenomenology of Little Higgs models at the Large Hadron Collider,* doi:10.22215/etd/2012-09748.

[45] T. A. W. Martin, *Examining extra neutral gauge bosons in non-universal models and exploring the phenomenology of the Bestest Little Higgs model at the LHC*, doi:10.22215/etd/2012-09697.

[46] S. P. Martin, *Adv. Ser. Direct. High Energy Phys.* **18**, 1 (1998).

[47] W. Hollik, J. I. Illana, S. Rigolin, C. Schappacher and D. Stockinger, *Nucl. Phys.* **B551**, 3 (1999); Erratum: *Nucl. Phys.* **B557**, 407 (1999).

[48] J. A. Aguilar-Saavedra, *Nucl. Phys.* **B812**, 181 (2009).

[49] E. Cruz-Albaro and A. Gutiérrez-Rodríguez, *Sensitivity limits on the weak dipole moments of the top-quark at the Bestest Little Higgs Model,* arXiv:2202.12738 [hep-ph].

[50] G. Aad, *et al.* (ATLAS Collaboration), *Eur. Phys. J.* **C81**, 396 (2021).

[51] S. Godfrey, T. Gregoire, P. Kalyniak, T. A. W. Martin and K. Moats, *JHEP* **04**, 032 (2012).

[52] M. A. Arroyo-Ureña, G. Hernández-Tomé and G. Tavares-Velasco, *Eur. Phys. J.* C **77**, 227 (2017).

[53] M. A. Arroyo-Ureña, G. Tavares-Velasco and G. Hernández-Tomé, *Phys. Rev.* D **97**, 013006 (2018).

[54] J. Bernabeu, D. Comelli, L. Lavoura and J. P. Silva, *Phys. Rev.* D **53**, 5222-5232 (1996).

[55] M. Arroyo-Ureña and E. Díaz, *J. Phys.* G **43**, 045002 (2016).

[56] A. Bolaños, A. Moyotl and G. Tavares-Velasco, *Phys. Rev.* D **89**, 055025 (2014).

[57] T. Ibrahim and P. Nath, *Phys. Rev.* D **78**, 075013 (2008).

[58] A. Moyotl and G. Tavares-Velasco, *Phys. Rev.* D **86**, 013014 (2012).

[59] C. Biggio, *Phys. Lett.* B **668**, 378-384 (2008).

[60] T. Huang, Z. H. Lin and X. Zhang, *Phys. Lett.* B **450**, 257-261 (1999).